Nonlinear Dynamics manuscript No.
(will be inserted by the editor)

Parametric Roll Vulnerability of Ships using Markov and Melnikov approaches

Abhilash Somayajula · Jeffrey Falzarano

Received: date / Accepted: date

Abstract The designs of modern container ships, roll-on roll-off (Ro-Ro) vessels and cruise vessels have evolved over the years and in recent times some of them have been observed to experience dynamic instabilities during operation in the open ocean. These catastrophic events demonstrate that satisfying prescriptive stability rules set forth by International Maritime Organization (IMO), national authorities (e.g. Coast Guard) and other classification societies are not sufficient to ensure dynamic stability of ships at sea. In light of these events, IMO is organizing efforts to make way towards a second generation of intact stability criteria that are better equipped to deal with these dynamic instabilities. This paper discusses the development of such a tool for parametric rolling in a realistic random seaway, which is one of the critical phenomena identified by IMO.

In this study, a previously developed analytical model for roll restoring moment, which was found to be effective in modeling the problem of parametric roll, is analyzed using the Melnikov approach. The stability of the system is quantified in terms of rate of phase space flux of the system. This approach is further compared with another technique known as the Markov approach that is based on stochastic averaging and quantifies stability in terms of mean first passage time. The sensitivity of both of these metrics to environmental parameters is investigated. Finally, the nature of random response is analyzed using Lyapunov exponents to determine if the vessel exhibits any chaotic dynamics.

Keywords Parametric Roll · Melnikov function · Volterra GZ method · Irregular seas · Rate of phase space flux · Stochastic Averaging · Lyapunov exponent · Markov approach · Nonlinear dynamical system · Global geometric method

A. Somayajula (Corresponding Author)
Department of Ocean Engineering, Indian Institute of Technology, Chennai, India - 600036
Tel.: +91-44-2257 4823
E-mail: s.abhilash89@gmail.com, abhilash@iitm.ac.in
Orcid ID: 0000-0002-5654-4627

J. Falzarano
Department of Ocean Engineering, Texas A & M University, College Station - 77843
E-mail: jfalzarano@civil.tamu.edu
Orcid ID: 0000-0002-8071-5588

1 Introduction

The last two decades have seen considerable advances in the ship design process resulting in newer hullforms. These newer designs enable larger amounts of cargo to be transported at higher speeds. An example of such a newer design is the modern container ship that is characterized by a fine underwater hull form to reduce resistance, a large flare and a broad stern to accommodate more containers on deck. Another example with similar design characteristics is the roll-on roll-off (RoRo) vessel used to transport automobiles across countries and continents. However, some of these newer designs have often been observed to exhibit unpredictable behavior in the open oceans that in many cases has led to severe damage to property, loss of life and sometimes both [11, 2].

A detailed investigation of some of these incidents has revealed that although these newer designs satisfied prescriptive static intact stability rules set forth by International Maritime Organization (IMO), they lacked dynamic stability [11]. Due to increased stability concerns of these newer designs, the IMO has decided to re-evaluate the current intact stability code and make way for a second generation of intact stability rules focusing on dynamic instabilities such as dead ship rolling, parametric rolling, surf riding and broaching [53].

The second generation stability assessment is further classified into three levels. Level 1 and Level 2 criteria involve empirical and semi-analytical assessments respectively and can be used to quickly ascertain if a design is safe or not. Level 3 involves direct stability assessment using time domain simulations (e.g. Somayajula and Falzarano (2015) [35]). While Level 3 is the most accurate it is also time consuming and cannot be used effectively to compare several interim design concepts investigated in preliminary design. Thus, there have been significant efforts to develop Level 2 criteria, which are proposed to help designers assess several designs quickly but at the same time are based on first principles and reflect underlying physics. Since simulations are time consuming and time is a big factor in assessing interim designs, analytical methods are appropriate for this problem.

One of the main challenges involved in developing an analytical stability criterion is to formulate a single degree of freedom system that can accurately model the phenomenon of parametric roll in irregular seas. The modeling of nonlinear time varying restoring moment in waves for single degree of freedom roll is a particularly hard problem and continues to be an active area of research. Some of the popular approaches include the Grim's effective wave approach and the Volterra $\overline{GM}$ method.

The Grim's effective wave approach approximates wave elevation in space by an equivalent regular wave and the roll restoring moment in random waves is obtained by interpolation from a precomputed lookup table of roll restoring moments in a range of regular waves. The Grim's effective wave formulation constrains the equivalent regular wave to have its crest aligned with the midship of the vessel. Later on, the Grim's effective wave was extended to overcome this constraint and have its crest at any position along the length of the hull depending on the random wave surface elevation [1]. Some of the limitations of the Grim's and the improved Grim's effective wave approaches include the inability to capture the effect of heave and pitch of the vessel on parametric roll and also a shifted peak of roll spectrum as compared to nonlinear coupled simulations [39].

The Volterra $\overline{GM}$ method on the other hand can include the effects of heave and pitch on the time varying metacentric height $\overline{GM}$ of a vessel in random sea [44, 27]. However, this method is limited to only capturing linear time varying stiffness and is found to over-predict the roll response. For a detailed comparison of these approaches, readers are referred to Somyajula and Falzarano (2017) [43]. To overcome the limitations of both models, a new analytical model called Volterra $\overline{GZ}$ method has been developed [39] and is utilized in this study. The Volterra $\overline{GZ}$ model is analyzed using the Melnikov function to come up with an analytical criterion to assess stability of any vessel to parametric roll in irregular seas. The results from this approach are also compared against another method previously developed by the authors that is based on the technique of stochastic averaging [40].

The rest of the paper is organized as follows. Section 2 discusses a review of the literature addressing related problems. A single degree of freedom model for parametric roll is introduced and described in section 3. Wave excitation and calculation of parametric excitation of the system are covered in section 4 and section 5 respectively. Section 6 discusses the concepts of phase plane and safe basin for a nonlinear dynamical system. It also discusses the geometric characteristics of the response in the presence of damping and regular excitation. The Melnikov function and its application to the problem of parametric roll of ship are discussed in section 7. Section 8 extends the Melnikov analysis to systems with random excitation and introduces the concept of the rate of phase space flux. Section 9 describes the Markov analysis that uses stochastic averaging to analyze the stability of the system. Section 10 compares the Markov and Melnikov approaches and discusses the sensitivity of each approach to environmental parameters. Section 11 discusses the characteristics of the random response by computing the Lyapunov exponents of the system. This is followed by conclusions reported in section 12.

2 Literature Review

Nonlinear roll response of a ship in irregular waves has been studied extensively in the past two centuries. Beginning with Froude [13] and Moseley [28] many researchers have investigated this problem to varying degrees of complexity. For a general floating vessel, all degrees of freedom are coupled to each other. However, using certain simplifying assumptions [55], roll motion can be shown to be decoupled from other modes of motion. This has led to analytical description of roll using a single degree of freedom equation of motion [7, 48].

Various methods have been developed to solve nonlinear roll equation of motion. The most intuitive approach is to obtain a numerical solution to the system assuming different initial conditions. Testing many initial conditions gives an idea of the nature of nonlinearity and its effect on the response. Thompson et al. (1992) [52] used this approach to study nonlinear roll motion in detail. Other investigators adopting this approach include Spyrou (1996) [46] and Virgin (1987) [54]. Although simulations help understand the system behavior, it is not practical to determine the effect of different parameters on system response using this approach. Due to the need to perform time consuming simulations for several initial conditions, this method is not practically applicable to analyze a set of designs in a short period of time.

Some approximate analytical approaches applied by researchers to overcome this limitation include multiple scale method [29], collocation approach and harmonic balance method (HBM) [23]. However, multiple scale method suffers from the limitation of being applicable to weakly nonlinear systems and is not effective for analyzing large angle roll motion. Similarly, HBM too suffers from a drawback that as nonlinearity of the problem increases, the number of secular terms increase and solving these large set of equations makes the problem untenable [21].

In contrast to the approaches described above, Guckenheimer and Holmes (1984) [15] (also Greenspan and Holmes (1984) [14] and Wiggins (1990) [56]) discussed the application of the *Melnikov method* (originally due to Melnikov [24]) to analyze complex dynamics exhibited by a nonlinear oscillator. Instead of obtaining numerical responses of a system, this approach focuses on the geometric behavior of critical solutions in the phase space. Due to its simplicity, generic nature and its capability to analyze strongly nonlinear systems this approach has become popular and is often used to analyze strongly nonlinear oscillators exhibiting complex chaotic dynamics. Falzarano (1990) [7] was one of the first researchers to apply this technique to investigate capsizing of a ship excited by regular beam seas.

The Melnikov method and many of the nonlinear dynamical system approaches were limited to systems that could be expressed as autonomous systems (systems with no external time varying forcing). Since only non-autonomous systems with a periodic excitation could be recast as an autonomous system of higher dimension [57], for a long time this method was limited to regular wave excitation. However, Frey and Simiu (1993) [12] extended the Melnikov approach to analyze systems with random excitation. They showed that the rate of phase space flux defined as the rate at which the area of safe basin (initial conditions leading to bounded solutions) is being transported out could be related to the area under the Melnikov function when it is non-negative. Hsieh et al. (1993) [16] used this approach to analyze the capsizing of a vessel in random beam seas. However, Hsieh et al. (1993) [16] approximated the frequency dependent radiation moment by considering added mass and radiation damping at the roll natural frequency. Jiang et al. (2000) [21] improved upon this model to consider the effect of frequency dependent radiation damping through a convolution integral.

While the Melnikov approach has been extensively used to analyze roll motion in beam sea, there is only limited literature discussing its application to parametric roll in head seas. Falzarano (1990) [7] briefly discussed parametrically excited roll motion in regular waves. A further detailed analysis of the behavior of manifolds for a parametrically excited roll motion for both biased (ship with a permanent list angle due to a negative metacentric height) and unbiased ships in regular waves was undertaken by Esparza and Falzarano (1993) [5]. Falzarano et al. (1993) [8] also looked at the problem of saturation induced roll motion in regular waves, where heave/pitch motions cause a time varying restoring force resulting in a parametrically excited roll motion. Moideen et al. (2013, 2014) studied the sensitivity of parametric roll to damping and forward speed using Ince-Strut diagrams [25,26]. However, all of the above studies on parametric excitation were limited to regular wave scenarios. Unlike for directly excited roll motion, there is very limited literature that discusses application of Melnikov approach to the problem of parametric roll in irregular waves. The extension of the Melnikov approach for parametrically excited systems is investigated in this paper.

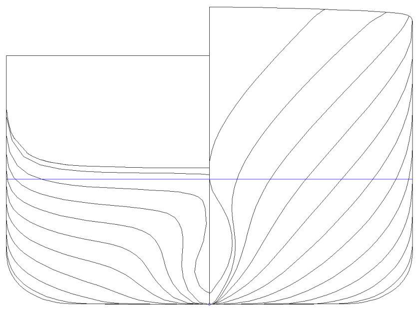

Fig. 1: Body plan of the C11 hull form

In contrast to the nonlinear dynamical systems approach, the stability of the system can also be analyzed using probabilistic methods. These include several class of methods including numerically solving the Fokker-Planck-Kolmogorov (FPK) equation [3], cumulant closure techniques [50,10] and stochastic averaging [31,51]. In general, most of these methods, including solving the FPK equation numerically and higher order cumulant closure techniques, are computationally expensive and cannot be used to analyze several designs in a short time. On the other hand, stochastic averaging is a simple technique that leads to a semi-analytical criterion in the form of a mean time for the system to fail. In this approach, equations of motion are averaged over one period of the unperturbed system response and this enables approximating the energy of the system as a Markov process. The mean first passage time for this Markov system is then computed by numerically solving the corresponding Pontryagin equations, which are a recursive set of boundary value differential equations for the moments of first passage time. The computation involved in solving the boundary value problem is minuscule. In this study the approach that approximates energy of the system as a Markov process will be referred to as the *Markov approach* or the *stochastic averaging* approach. In a previous study, authors have already implemented and analyzed the roll response of a ship subjected to random parametric excitation using the Markov approach [40]. In this paper we compare the results from the Melnikov approach to the results from the Markov approach to understand the sensitivity of both methods to system parameters.

The modified C11 container ship hull, which is known to be vulnerable to parametric excitation [11] is chosen for analysis in this paper. The body plan of the vessel is shown in Figure 1 and its particulars are listed in Table 1.

3 State Space Formulation

The single degree of freedom equation governing the roll motion of a vessel experiencing head on waves is given by (1)

$$\begin{aligned}[I_{44} + A_{44}(\infty)]\phi'' + \int_{-\infty}^{u} K_{44}(u-v)\phi'(v)dv + B_1\phi' \\ + B_2\phi'|\phi'| + \rho g \nabla_0 \overline{GZ}(u,\phi) = 0 \end{aligned} \quad (1)$$

Table 1: Details of the C11 hull form

Particulars	**Value**
Length between perpendiculars L_{pp} (m)	262.00
Breadth B (m)	40.00
Depth D (m)	24.45
Mean Draft T (m)	12.32
Displacement $\Delta = \rho\nabla$ (tonnes)	76056.00
Vertical Center of Gravity $\overline{KG}$ (m)	18.32
Metacentric Height $\overline{GM}$ (m)	1.973
Roll Natural Period T_n (sec)	22.78
Forward Speed of the Vessel U (knots)	8.00

where

$\phi(u)$ is roll angle which is a function of time u
ϕ' is first derivative of roll angle with respect to u
ϕ'' is second derivative of roll angle with respect to u
I_{44} is mass moment of inertia of the vessel
$A_{44}(\infty)$ is added mass moment of inertia of the vessel at infinite frequency
$K_{44}(\tau)$ is roll impulse response function (IRF)
B_1 is viscous linear roll damping coefficient
B_2 is viscous quadratic roll damping coefficient
∇_0 is calm water displacement of the vessel
$\overline{GZ}(u,\phi)$ is time varying roll restoring arm in the presence of waves
ρ denotes density of sea water and has a value of 1025 kg/m^3
g denotes acceleration due to gravity and has a value of 9.81 m/s^2

Typically for ships the roll radiation damping is small and hence viscous effects play an important role and need to be included for accurate modeling. The linear and quadratic damping coefficients are usually computed from free decay experiments. However, free decay tests are performed in calm waters and do not necessarily capture the damping in waves [37]. One can overcome this limitation by performing forced oscillation tests and extracting the damping coefficients using system identification techniques [36,38]. In the absence of experimental data, linear and quadratic viscous roll damping coefficients are calculated by the standard Ikeda approach [19]. In this study Ikeda approach is adopted to calculate the viscous damping coefficients and the details of this empirical method are provided in Falzarano et al. (2015) [6].

The time varying roll restoring arm $\overline{GZ}(u,\phi)$ in waves can be expressed as the sum of the calm water roll restoring arm $\overline{GZ}_0(\phi)$ and the time varying component $\Delta\overline{GZ}(u,\phi)$ as shown below

$$\overline{GZ}(u,\phi) = \overline{GZ}_0(\phi) + \Delta\overline{GZ}(u,\phi) \tag{2}$$

Since most ship hulls have a port-starboard symmetry, the roll restoring arm $\overline{GZ}_0(\phi)$ can be expressed as an odd polynomial of roll angle ϕ with constant coefficients. Similarly, the time varying component of roll restoring moment $\Delta\overline{GZ}(u,\phi)$ can also be expressed as an odd polynomial of roll angle but with time varying coefficients. Thus, the time varying roll restoring arm in waves $\overline{GZ}(u,\phi)$ can be

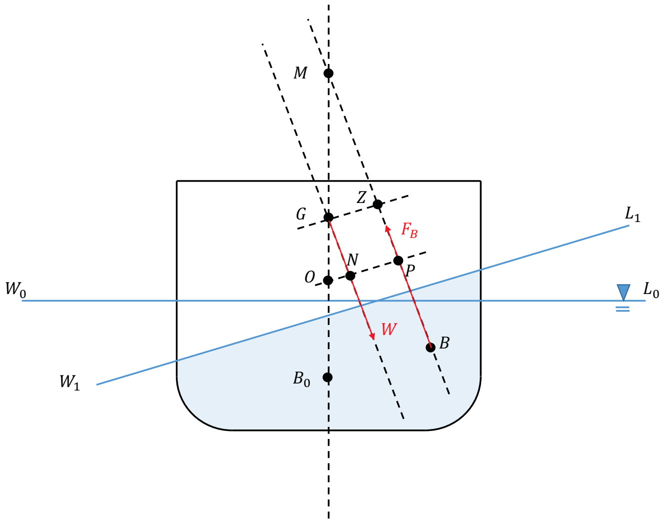

Fig. 2: Roll restoring moment in waves

expressed as

$$\begin{aligned}\overline{GZ}(u,\phi) = (K_1^{(0)} + K_1^{(1)}(u))\phi + (K_3^{(0)} + K_3^{(1)}(u))\phi^3 \\ + (K_5^{(0)} + K_5^{(1)}(u))\phi^5 + ...\end{aligned} \quad (3)$$

where $K_i^{(0)}$ $(i = 1, 3, 5, ...)$ are the time invariant coefficients corresponding to the calm water roll restoring arm $\overline{GZ}_0(\phi)$ and $K_i^{(1)}(u)$ $(i = 1, 3, 5, ...)$ are the time varying coefficients corresponding to the time varying component of the roll restoring arm $\Delta\overline{GZ}(u, \phi)$. The calculation of $K_i^{(1)}(u)$ $(i = 1, 3, 5, ...)$ is discussed in section 5.

The linear coefficient $K_1^{(0)}$ is well known as the metacentric height in naval architecture terminology and is denoted by $\overline{GM}_0$. The metacentric height represents the vertical distance between the center of gravity of the vessel and its metacenter and is a measure of the initial static roll restoring stiffness of the vessel. When a vessel undergoes a roll motion (about an axis passing through O) as shown in Figure 2, the position of center of the buoyancy changes (from B_0 to B) due to a change in underwater hull geometry. The metacenter M is the point where the line of action of buoyancy force in the heeled condition intersects with the line of action of the buoyancy force in the upright condition. In Figure 2, W_0L_0 represents the calm waterline in the upright condition and W_1L_1 represents the dynamic waterline in a heeled condition and in the presence of waves. M_0 represents the limiting position of the metacenter M when the vessel is floating in an upright condition and in calm water. Thus, the time varying roll restoring arm in waves $\overline{GZ}(u, \phi)$

can be expressed as

$$\overline{GZ}(u,\phi) = \overline{GM}_0 \frac{\overline{GZ}(u,\phi)}{\overline{GM}_0} \tag{4}$$

$$\begin{aligned} &= \overline{GM}_0 \left[\left(\phi + \frac{K_3^{(0)}}{\overline{GM}_0}\phi^3 + \frac{K_5^{(0)}}{\overline{GM}_0}\phi^5 + ... \right) \right. \\ &\left. + \left(\frac{K_1^{(1)}(u)}{\overline{GM}_0}\phi + \frac{K_3^{(1)}(u)}{\overline{GM}_0}\phi^3 + \frac{K_5^{(1)}(u)}{\overline{GM}_0}\phi^5 + ... \right) \right] \end{aligned} \tag{5}$$

$$\begin{aligned} &= \overline{GM}_0 \left[\left(\phi + \alpha_3\phi^3 + + \alpha_5\phi^5 + ... \right) \right. \\ &\left. + \left(k_1(u)\phi + k_3(u)\phi^3 + k_5(u)\phi^5 + ... \right) \right] \end{aligned} \tag{6}$$

where $\alpha_i = \frac{K_i^{(0)}}{\overline{GM}_0}$ and $k_i(u) = \frac{K_i^{(1)}(u)}{\overline{GM}_0}$ for $i = 1, 3, 5, ...$ For small angles of motion the effect of higher order restoring terms in (6) can be neglected and the undamped natural frequency ω_n of the resulting linearized system is given by

$$\omega_n = \sqrt{\frac{\rho g \nabla_0 \overline{GM}_0}{I_{44} + A_{44}(\omega_n)}} \tag{7}$$

where $A_{44}(\omega_n)$ represents the frequency dependent roll added mass moment of inertia evaluated at ω_n. In the case of a parametrically excited system, it is well known that the subharmonic response of nonlinear system shown in (1) is narrow banded around the linear roll natural frequency of the vessel ω_n. Therefore, it is reasonable to approximate the roll radiation moment by the added mass and radiation damping terms evaluated at the undamped roll natural frequency instead of a convolution integral shown in (1). This leads to the simplification shown in (8).

$$\begin{aligned} [I_{44} + A_{44}(\omega_n)]\phi'' &+ (B_{44}(\omega_n) + B_1)\phi' + B_2\phi'|\phi'| \\ &+ \rho g \nabla_0 \overline{GM}_0 \left[\left(\phi + \alpha_3\phi^3 + + \alpha_5\phi^5 + ... \right) \right. \\ &\left. + \left(k_1(u)\phi + k_3(u)\phi^3 + k_5(u)\phi^5 + ... \right) \right] = 0 \end{aligned} \tag{8}$$

This equation in terms of non-dimensional time t is given by (9)

$$\begin{aligned} \ddot{x} + \epsilon\delta_1\dot{x} + \epsilon\delta_2\dot{x}|\dot{x}| &+ \left[x + \alpha_3 x^3 + \alpha_5 x^5 + ... \right] \\ &+ \left[\epsilon p_1(t)x + \epsilon p_3(t)x^3 + \epsilon p_5(t)x^5 + ... \right] = 0 \end{aligned} \tag{9}$$

where

$$x = \phi \qquad t = \omega_n u \qquad \dot{(\ )} = \frac{d}{dt}(\ ) = \frac{1}{\omega_n}\frac{d}{du}(\ ) \tag{10}$$

$$\epsilon\delta_1 = \frac{B_1 + B_{44}(\omega_n)}{[I_{44} + A_{44}(\omega_n)]\omega_n} \tag{11}$$

$$\epsilon\delta_2 = \frac{B_2}{[I_{44} + A_{44}(\omega_n)]} \tag{12}$$

$$\epsilon p_1(t) = k_1\left(\frac{t}{\omega_n}\right) \qquad \epsilon p_3(t) = k_3\left(\frac{t}{\omega_n}\right) \qquad \epsilon p_5(t) = k_5\left(\frac{t}{\omega_n}\right) \qquad ... \tag{13}$$

Note that a small parameter ϵ is introduced to represent the relative order of various terms in the equation of motion. The relative order indicates that terms proportional to ϵ^0 govern the global geometrical characteristics of the system and the effect of excitation and damping on global geometrical characteristics is of the order of ϵ. Excitation and damping being proportional to ϵ does not imply that the system and the developed methods are applicable to only small excitation or damping. However, it is assumed that excitation and damping do not drastically alter the global geometry of solutions.

The system can further be expressed in state space form as shown in (14) and (15) where $y = \dot{x}$. It can be seen that the time varying perturbation is $O(\epsilon)$ and the system can be thought of as a Hamiltonian system with small perturbations.

$$\dot{x} = y \tag{14}$$

$$\dot{y} = -\Big[x + \alpha_3 x^3 + \alpha_5 x^5 + ...\Big] + \epsilon\left\{ -\delta_1\dot{x} - \delta_2\dot{x}|\dot{x}| - \Big[p_1(t)x + p_3(t)x^3 + p_5(t)x^5 + ...\Big]\right\} \tag{15}$$

The Hamiltonian E of the system represents the sum of kinetic and potential energies of unperturbed system and is given by

$$E = \frac{\dot{x}^2}{2} + U(x) = \frac{\dot{x}^2}{2} + \frac{x^2}{2} + \alpha_3\frac{x^4}{4} + \alpha_5\frac{x^6}{6} + ... \tag{16}$$

4 Wave Excitation

It is assumed that wave elevation in the ocean can be regarded as a zero mean Gaussian process and is characterized by a Bretschneider spectrum given by

$$S(\omega) = \frac{5T_pH_s^2}{32\pi}\left(\frac{2\pi}{\omega T_p}\right)^5 e^{-\frac{5}{4}\left(\frac{2\pi}{\omega T_p}\right)^4} \tag{17}$$

where H_s is the significant wave height defined as the average wave height of the highest one third of the waves and T_p is the peak period defined as the period corresponding to peak of the spectrum. For a vessel moving with forward speed V_0, the apparent frequency of a wave (perceived by an observer on the vessel) differs from the actual frequency of the wave due to the Doppler effect. This apparent frequency is known as the encounter frequency ω_e of the wave and is related to the original wave frequency ω by

$$\omega_e = \omega - kV_0\cos(\beta) \tag{18}$$

where β is the wave direction measured relative to the longitudinal axis of the ship in a counter clockwise direction and k is the wave number of incident wave. In deep waters, the wave number k and wave frequency ω are related by the dispersion relation given by $\omega^2 = gk$. Thus, the encounter frequency is expressed as

$$\omega_e = \omega - \frac{\omega^2 V_0}{g}\cos(\beta) \tag{19}$$

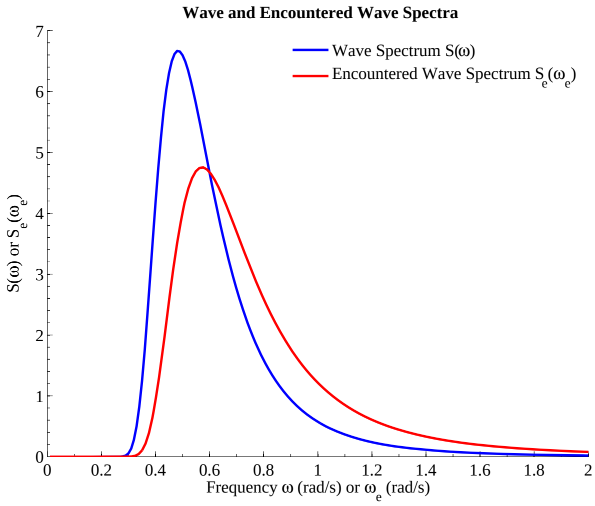

Fig. 3: Wave and encounter wave spectra

Thus for an observer on board a ship, the encounter spectrum $S_e(\omega_e)$ of waves can be obtained by equating the energy under the original and the encountered wave spectra as shown below.

$$S_e(\omega_e)|d\omega_e| = S(\omega)|d\omega| \tag{20}$$

$$S_e(\omega_e) = S(\omega)\left|\frac{d\omega}{d\omega_e}\right| = \frac{S(\omega)}{\left|1-\frac{2V_0\omega}{g}\cos(\beta)\right|} \tag{21}$$

The Bretschneider wave spectrum for $H_s = 6\ m$ and $T_p = 13\ sec$ and the corresponding encountered wave spectrum for a forward speed $V_0 = 8\ knots$ and head on condition ($\beta = 180^0$) are shown in Figure 3. For head seas, the encounter frequency of an incident wave is higher than the actual frequency of the wave. Hence in Figure 3, the peak of the encountered wave spectrum is shifted to the right.

A wave elevation record of length U_{max} with a sampling interval of Δu can be obtained by employing the random phase method. In the random phase method the encountered wave spectrum $S_e(\omega_e)$ is first computed at $N = \frac{U_{max}}{2\Delta u}$ discrete frequencies $\omega_m = (m-1)\Delta\omega_e$ $(m = 1, 2, ..., N)$ with a uniform spacing of $\Delta\omega_e = \frac{2\pi}{U_{max}}$. The wave elevation record is approximated by a linear superposition of N harmonic components as shown below

$$\eta(u,x,y) = \frac{1}{2}\sum_{m=1}^{N} a_m \Big[e^{i\{-k_m(x\cos(\beta)+y\sin(\beta))+\omega_m u+\varepsilon_m\}} + e^{-i\{-k_m(x\cos(\beta)+y\sin(\beta))+\omega_m u+\varepsilon_m\}}\Big] \tag{22}$$

where

$a_m = \sqrt{2S_e(\omega_m)\Delta\omega_e}$ is the amplitude of the m^{th} harmonic component

ω_m is the encounter frequency of the m^{th} harmonic component
k_m is the wave number of the m^{th} harmonic component
ε_m is the phase of the m^{th} harmonic component and is realized by sampling a uniform random variable in $[0\ 2\pi)$

For a head sea condition $\beta = \pi$ and the wave elevation is given by

$$\eta(u,x) = \frac{1}{2}\sum_{m=1}^{N} a_m \left[e^{i\{-k_m x+\omega_m u+\varepsilon_m\}} + e^{-i\{-k_m x+\omega_m u+\varepsilon_m\}}\right] \tag{23}$$

5 Parametric Excitation - The Volterra $\overline{GZ}$ Method [39]

The coefficients of the time varying components of the roll restoring arm $K_i^{(1)}(u)$ $(i = 1,3,5,...)$ in (3) have a nonlinear dependence on following factors:

- The geometry of vessel
- The instantaneous position and orientation of vessel
- The spatial wave field around the vessel

These factors make analytical modeling of the roll restoring arm in the presence of waves particularly challenging. Several approaches have been suggested over the years to approximately model the roll restoring arm in irregular waves [41,45]. In this study, the Volterra $\overline{GZ}$ method is adopted that directly results in a set of first order Volterra transfer functions $f_i(\omega_e)$ for each $K_i^{(1)}(u)$ $(i = 1,3,5,...)$. Time varying coefficients $K_i^{(1)}(u)$ $(i = 1,3,5,...)$ can then be calculated as shown in (24) where $f_i^*(\omega_m)$ is complex conjugate of $f_i(\omega_m)$.

$$K_i^{(1)}(u) = \frac{1}{2}\sum_{m=1}^{N} a_n \left[f_i(\omega_m)e^{i\{\omega_m u+\varepsilon_m\}} + f_i^*(\omega_m)e^{-i\{\omega_m u+\varepsilon_m\}}\right] \tag{24}$$

In addition to first order transfer functions, the Volterra $\overline{GZ}$ method also provides expressions for higher order transfer functions. The contributions of higher order components decrease significantly as the order of transfer function increases. This will also be shown in section 7. Therefore, in this study we will evaluate $K_i^{(1)}(u)$ $(i = 1,3,5,...)$ using only the first order Volterra $\overline{GZ}$ transfer functions $f_i(\omega_e)$.

To calculate the Volterra transfer functions for roll restoring arm, the ship hull is divided into a set of transverse strips along the length of hull. The hydrostatic restoring moment at each section is expressed as a Taylor series expansion about the restoring moment at the mean draft. Contributions of each section are then integrated longitudinally to yield the transfer function. For brevity, a detailed derivation of Volterra $\overline{GZ}$ transfer functions and other modeling details are not provided here and the interested readers are referred to Somayajula and Falzarano (2018) [39] or Somayajula (2017) [42] for details. The Volterra $\overline{GZ}$ transfer functions for the modified C11 container ship are shown in Figure 4.

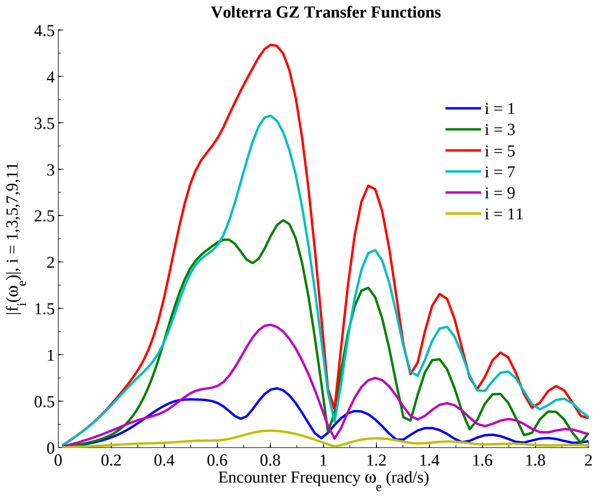

Fig. 4: Volterra $\overline{GZ}$ transfer functions for C11 hullform

6 The Phase Plane and the Concept of Safe Basin

The unperturbed system ($\epsilon = 0$) represents an unforced and undamped system and is given by (25) and (26).

$$\dot{x} = y \tag{25}$$

$$\dot{y} = -\left[x + \alpha_3 x^3 + \alpha_5 x^5 + ...\right] \tag{26}$$

The solutions of the unperturbed system in the (x, y) phase plane are shown in Figure 5. *Fixed* or *equilibrium* points of the system are defined as the points in the phase plane where $\dot{x} = 0$ and $\dot{y} = 0$. The system described by (25) and (26) has three fixed points - one center at $(0, 0)$ corresponding to the upright condition and two saddle points $(\pm x_v, 0)$ corresponding to the angle on vanishing stability. The two saddle points are connected by two symmetric orbits known as *heteroclinic orbits*. When the system starts with an initial condition inside the region bounded by the heteroclinic orbits, the response is oscillatory and bounded. This region is therefore known as the *safe basin* of the unperturbed system. For all initial conditions outside the safe basin, the response is unbounded and leads to capsize or escape. The heteroclinic orbits form the basin boundary and separate regions with bounded and unbounded responses. Therefore, the heteroclinic orbits forming the basin boundary are also known as *separatrices*. These heteroclinic orbits are also invariant manifolds as when the system starts with an initial condition on one of these orbits, the response continues to stay on the same orbit for all future and past times [56].

Introducing damping or excitation (not necessarily harmonic or periodic) results in separation of the heteroclinic orbits. A time varying excitation leads to a time varying position of fixed points in the phase plane. If the excitation is periodic, then both the position of fixed point and the vector field given by (14) and (15) will be same at any two times separated by one period of the excitation.

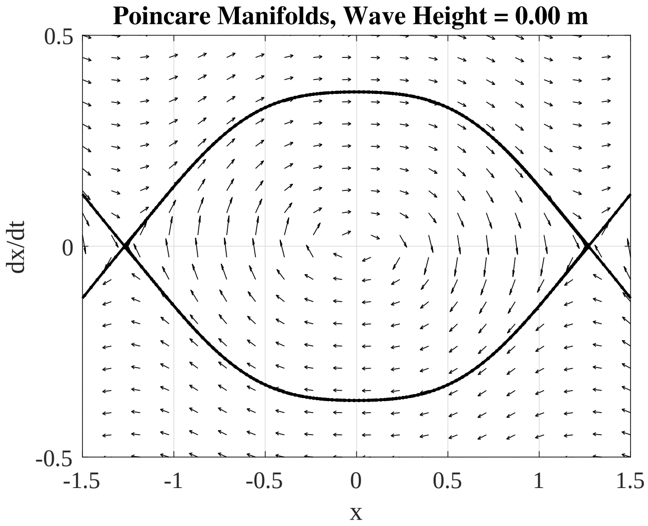

Fig. 5: Phase plane for the unperturbed system

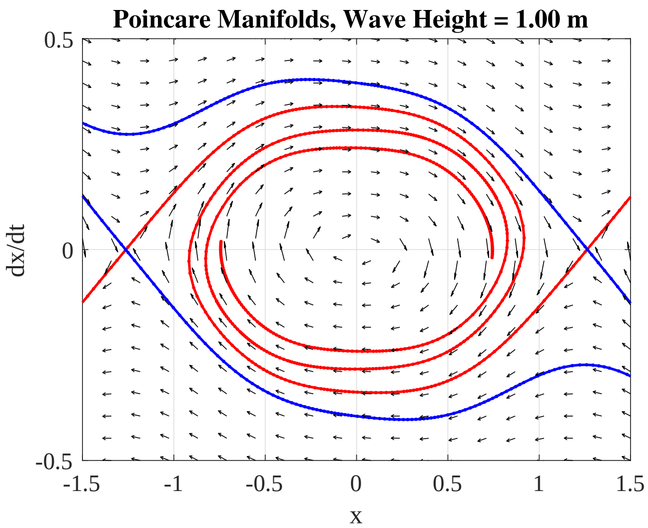

Fig. 6: Numerically computed Poincaré manifolds for ship roll system subjected to regular wave of height $H = 1.0\ m$ and period $T = 10\ sec$ (stable and unstable manifolds are shown in blue and red respectively)

Thus, fixed points are transformed into periodic orbits and the position of the heteroclinic orbits oscillate periodically in time.

Stroboscopically sampling the phase plane at specific times separated by one period of excitation provides a unique insight into the dynamics of the system. This discrete map of the system is known as a Poincaré map named after Henri Poincaré who originally introduced this technique and used it to study several nonlinear

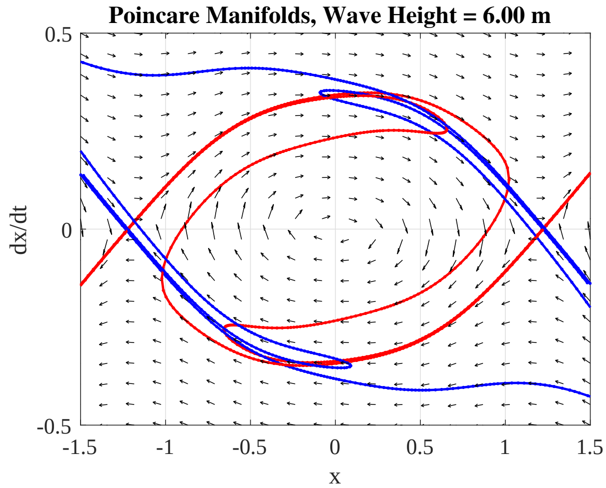

Fig. 7: Numerically computed Poincaré manifolds for ship roll system subjected to regular wave of height $H = 6.0\ m$ and period $T = 10\ sec$ (stable and unstable manifolds are shown in blue and red respectively)

dynamical systems. A consequence of this discrete sampling is that periodic orbit traced by a fixed point of the unperturbed map due to a periodic excitation appears as a fixed point on a Poincaré map. Similarly, heteroclinic orbits whose position varies periodically with time appear as fixed curves on a Poincaré map. Heteroclinic orbits of the roll system of the modified C11 hull form subjected to regular head on waves are shown in Figure 6. The numerical computation of Poincaré manifolds has been performed by implementing the algorithm described by Parker and Chua (1989) [30]. The blue curves denote the stable manifolds and the red curves denote the unstable manifolds. The bounded region between the two blue stable manifolds are the set of initial conditions which when iterated in time will converge to the fixed point at $(0, 0)$.

When the excitation level is increased beyond a critical level, the separated heteroclinic manifolds intersect transversely with each other. Since heteroclinic orbits are also invariant manifolds, any forward or backward iteration of the intersection point will also lie on both manifolds. This means that the stable and unstable manifolds will have infinite transverse intersections. These intersections lead to the formation of lobes of phase space entrapped between the two manifolds. These lobes of initial conditions exhibit complicated dynamics that creates a possibility for solutions near the separatrices to be transported out of the safe basin. Such transitions usually may lead to the occurrence of chaotic responses and even capsize [9, 52, 54]. Figure 7 only shows a few intersection points between stable and unstable manifolds due to the finite length of manifolds computed using the numerical scheme. In theory if the manifolds are fully computed then they will intersect over and over infinite number of times.

Wiggins [56, 57] discusses chaotic responses to harmonically excited systems using Poincaré maps in detail. When the excitation (direct or parametric) is random then eventually at some time the excitation will be large enough to cause the intersection of the stable and unstable manifolds and transport from the safe to unsafe region will occur. It is important to note that in the case of random excitation, the vector field is no longer periodic, which means that the invariant manifolds can no longer be visualized using Poincaré maps as seen in Figure 6 and Figure 7.

Even in case of random excitation, the mechanism of transport of solutions from safe to unsafe regions occurs because of the intersections between stable and unstable manifolds. Melnikov (1963) [24] came up with a simple analytical function to calculate the transverse distance between manifolds. This distance given by the Melnikov function can be calculated even in case of random excitation when the manifolds themselves cannot be visualized. This opened the door for further study of dynamics of nonlinear dynamical systems excited by random excitation [12].

7 Melnikov Function

The separation distance $d(t_0)$ between the stable and unstable manifolds to $O(\epsilon)$ is defined as the Melnikov function and is given by (28)

$$d(t_0) = \epsilon M(t_0) + O(\epsilon^2) \tag{27}$$

$$M(t_0) = \int_{-\infty}^{\infty} y_0(t)\Bigg\{ - \delta_1 y_0(t) - \delta_2 y_0(t)|y_0(t)| - \Big[p_1(t+t_0)x_0(t) + p_3(t+t_0)x_0^3(t) + p_5(t+t_0)x_0^5(t) + ...\Big] \Bigg\}dt \tag{28}$$

where $x_0(t)$ and $y_0(t)$ are solutions representing the separatrices of the unperturbed system (Eqns. (25) and (26)). The theoretical proof that the Melnikov function represents the separation distance to $O(\epsilon)$ can be found in classical texts on nonlinear dynamical systems [15,56]. The Melnikov function can be separated into two parts - the time invariant mean component $\overline{M}$, which depends on damping and the time varying oscillatory part $\tilde{M}(t_0)$, which depends on excitation.

$$M(t_0) = \overline{M} + \tilde{M}(t_0) \tag{29}$$

where

$$\overline{M} = \int_{-\infty}^{\infty} y_0(t)\Bigg\{ - \delta_1 y_0(t) - \delta_2 y_0(t)|y_0(t)| \Bigg\}dt \tag{30}$$

$$\tilde{M}(t_0) = \int_{-\infty}^{\infty} y_0(t)\Big\{ - \Big[p_1(t+t_0)x_0(t) + p_3(t+t_0)x_0^3(t) + p_5(t+t_0)x_0^5(t) + ...\Big] \Big\}dt \tag{31}$$

The oscillatory component can further be expressed as

$$\tilde{M}(t_0) = \tilde{M}_{p_1}(t_0) + \tilde{M}_{p_3}(t_0) + \tilde{M}_{p_5}(t_0) + ... \tag{32}$$

where

$$\tilde{M}_{p_1}(t_0) = -\int_{-\infty}^{\infty} y_0(t)x_0(t)p_1(t+t_0)dt \tag{33}$$

$$\tilde{M}_{p_3}(t_0) = -\int_{-\infty}^{\infty} y_0(t)x_0^3(t)p_3(t+t_0)dt \tag{34}$$

$$\tilde{M}_{p_5}(t_0) = -\int_{-\infty}^{\infty} y_0(t)x_0^5(t)p_5(t+t_0)dt \tag{35}$$

For systems with only direct excitation and no parametric excitation, the oscillatory component of the Melnikov function is a linear function of the roll excitation moment [7,16,21,49]. However, for parametric excitation, $\tilde{M}(t_0)$ is a sum of stochastic processes as shown in (32).

It can be seen from (30) and (31) that evaluation of the Melnikov function requires only a knowledge of the closed form solution of the unperturbed system $(x_0(t), y_0(t))$. Therefore this method can be used to analyze the global geometry of solutions of the system even when the instantaneous response (x, y) itself is unknown.

Typically, a cubic restoring model is used to model the restoring moment in directly excited systems and has been applied to the problem of ship rolling in beam seas [9,17]. However, only a few researchers have investigated analytical studies with restoring models of fifth or higher degrees of polynomial [18,33]. For a system with up to 5^{th} degree of restoring terms, it is still possible to get an analytical expression for $(x_0(t), y_0(t))$ [18]. For systems with a higher degree of restoring terms, one cannot obtain a specific class (hyperelliptic) of solutions for the unperturbed system trajectories $(x_0(t), y_0(t))$ [47] and hence need to be evaluated numerically [7].

Somayajula and Falzarano (2018) [39] suggest that ideally a 9^{th} or 11^{th} degree polynomial is appropriate to represent the nonlinear roll stiffness. However, due to the lack of closed form analytical expressions, much of the literature is limited to 3^{rd} or at most 5^{th} degree representations. While 3^{rd} degree polynomial approximation enables capturing a softening stiffness, a 5^{th} degree representation is required to capture initial hardening and eventual softening of a typical righting arm curve for wall sided ships. This effect of initial hardening and eventual softening is more enhanced when the righting arm is calculated for the condition of wave crest at the midship and is shown in Figure 8 for the modified C11 hull form. The variation in $\overline{GZ}$ due to the location of the wave crest relative to the ship hull is shown in Figure 9. As the wave crest moves away from midship leading to the situation of the trough at midship, the initial hardening effect is less pronounced. However to accurately capture both cases one must use at least a 5^{th} degree representation. In this study, a 11^{th} degree polynomial restoring term is be used to represent the nonlinear roll restoring moment. Since no closed form analytical solutions are available, the unperturbed solutions in this study are evaluated numerically.

As previously discussed, the Volterra $\overline{GZ}$ method provides transfer functions for computing the varaition of $\overline{GZ}(t)$ up to various orders of relative wave elevation (taking into account the effect of heave and pitch motions of the vessel). As in the basic design phase a designer is more interested in evaluating various competing designs rather than absolute stability, which is almost always ascertained through simulations, we restrict the study to using only the $1st$ order $\overline{GZ}$ varaition. This

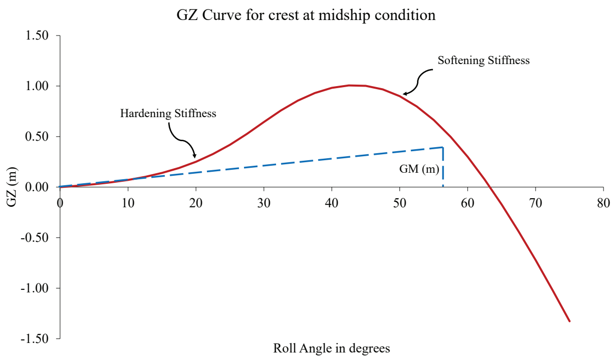

Fig. 8: $\overline{GZ}$ curve of Pram hull in case of wave crest at midship

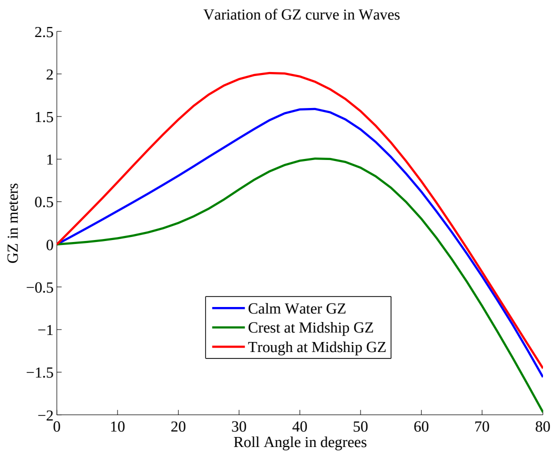

Fig. 9: $\overline{GZ}$ curve variation in waves

way the linear relationship between the excitation and Melnikov function can be utilized to speed up computation of the vulnerability criterion. Also it will be shown later that the effect of including the higher order transfer functions is not too significant.

It can be seen from (33 - 35) that each of the components of the oscillatory part of the Melnikov function $\tilde{M}_{p_i}(t_0)$ for $i = 1, 3, 5, ...$ are linear functions of the parametric excitations $p_i(t)$ for $i = 1, 3, 5, ...$ respectively. Under the assumption that the wave elevation is a zero mean ergodic Gaussian process, it follows that $p_i(t)$ for $i = 1, 3, 5, ...$ evaluated using first order Volterra transfer functions will also be zero mean ergodic Gaussian processes. Since $\tilde{M}_{p_i}(t_0)$ for $i = 1, 3, 5, ...$ are linear functions of parametric excitations $p_i(t)$ for $i = 1, 3, 5, ...$, it also follows that $\tilde{M}_{p_i}(t_0)$ for $i = 1, 3, 5, ...$ are ergodic Gaussian processes. As $\tilde{M}(t_0)$ is a sum of Gaussian random variables $\tilde{M}_{p_i}(t_0)$ for $i = 1, 3, 5, ...$, it has a Gaussian distribution

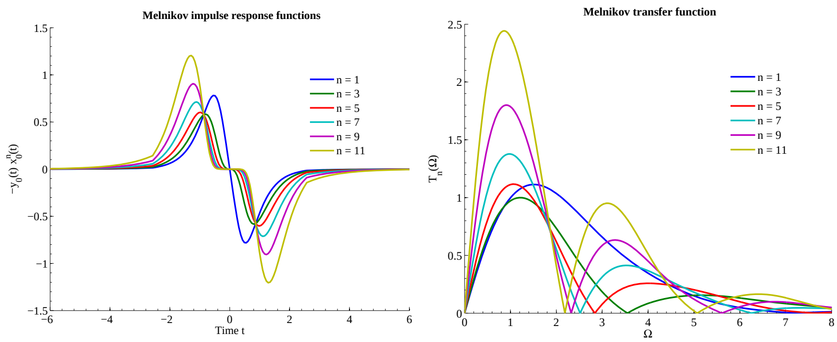

(a) Time domain impulse response (b) Frequency domain transfer function

Fig. 10: Melnikov function impulse response and frequency domain transfer functions

as well. The spectrum of $\tilde{M}(t_0)$ expressed as $S_{\tilde{M}\tilde{M}}(\Omega)$ is given by

$$S_{\tilde{M}\tilde{M}}(\Omega) = \sum_{j=1,3,5,\dots}^{N_q} \sum_{k=1,3,5,\dots}^{N_q} S_{\tilde{M}_{p_j}\tilde{M}_{p_k}}(\Omega) \tag{36}$$

where N_q is the degree of stiffness considered in the Volterra Model and cross spectra $S_{\tilde{M}_{p_j}\tilde{M}_{p_k}}(\Omega)$ are given by

$$S_{\tilde{M}_{p_j}\tilde{M}_{p_k}}(\Omega) = (2\pi)^2 \bar{T}_j(\Omega) T_k(\Omega) S_{p_j p_k}(\Omega) \tag{37}$$

$$= \epsilon^2 (2\pi)^2 \bar{T}_j(\Omega) T_k(\Omega) \bar{f}_j(\Omega) f_k(\Omega) S_{\eta\eta}(\Omega) \tag{38}$$

where $\bar{()}$ represents the complex conjugate, $\Omega = \frac{\omega_e}{\omega_n}$ is the scaled encounter frequency and $S_{\eta\eta}(\Omega)$ is the encountered wave spectrum, f_j represent the first order Volterra transfer functions described in section 5. The transfer function T_j is the Fourier transform of $-y_0(t)x_0^j(t)$ and is given by (39). The impulse response functions $-y_0(t)x_0^j(t)$ and their corresponding frequency domain transfer functions $T_j(\Omega)$ for $j = 1, 3, 5, \dots$ are shown in Figure 10.

$$T_j(\Omega) = \frac{1}{2\pi} \int_{-\infty}^{\infty} -y_0(t) x_0^j(t) e^{-i\Omega t} dt \tag{39}$$

Since each of the components of the oscillatory part of the Melnikov function have zero mean, $\tilde{M}$ is also a zero mean ergodic Gaussian process. The mean square value of $\tilde{M}$ is given by

$$\sigma_{\tilde{M}}^2 = E[\tilde{M}^2(t_0)] = \int_0^\infty S_{\tilde{M}\tilde{M}}(\Omega) d\Omega$$

$$= \epsilon^2 (2\pi)^2 \sum_{j=1,3,5,\dots}^{N_q} \sum_{k=1,3,5,\dots}^{N_q} \int_0^\infty \bar{T}_j(\Omega) T_k(\Omega) \bar{f}_j(\Omega) f_k(\Omega) S_{\eta\eta}(\Omega) d\Omega \tag{40}$$

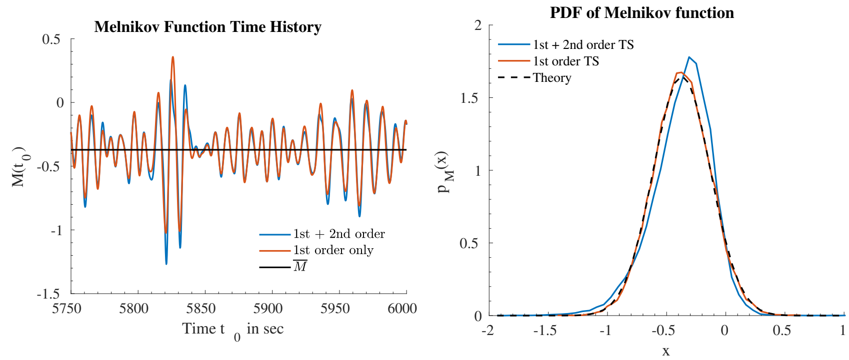

(a) 400 second window of time history

(b) Probability density function

Fig. 11: Melnikov function time histories and probability density function for $H_s = 6\ m$ and $T_p = 13\ sec$

Since a Gaussian distribution of a process is characterized by its mean and standard deviation, the probability density function of $\tilde{M}$ is given by

$$p_{\tilde{M}}(x) = \frac{1}{\sqrt{2\pi}\sigma_{\tilde{M}}} \exp\left(-\frac{x^2}{2\sigma_{\tilde{M}}^2}\right) \tag{41}$$

where $p_{\tilde{M}}(x)dx$ represents the probability of the random variable $\tilde{M}(t) \in [x, x+dx]$. A 400 second section of a 3-hour Melnikov function time history for $H_s = 6\ m$ and $T_p = 13\ sec$ is shown in Figure 11a. Figure 11b shows the comparison of empirical probability density functions obtained from time histories with the Gaussian probability density function.

Using only the $1st$ order Volterra $\overline{GZ}$ transfer function, leads to a Gaussian distribution of the Melnikov function. Using both $1st$ and $2nd$ order Volterra $\overline{GZ}$ transfer functions leads to a slight skew of the probability density function of the Melnikov function. However, the deviation from Gaussian distribution is small, indicating that the effect of neglecting higher orders of Volterra $\overline{GZ}$ transfer functions is not too significant.

8 Phase Space Flux

By definition, a negative value of the Melnikov function $M(t_0) < 0$ indicates that the stable manifold lies outside the unstable manifold as depicted in Figure 6. If for a system the unstable manifold lies outside the stable manifold for all times, then all the solutions with initial conditions outside the boundary will be unstable and lead to capsize. In this case the Melnikov function $M(t_0) > 0$ for all times. An unforced system with a negative damping coefficient is an example where the Melnikov function will always be greater than zero.

However, the more commonly encountered case is the multiple intersections of the stable and unstable manifolds caused by higher levels of excitation leading to continual switching of the relative orientations of the stable and unstable manifolds. This leads to the possibility of safe initial conditions near the boundary to be transported into the unsafe regions at some future time. The dynamics of these lobes of phase space with switching boundaries is described in more detail by Wiggins (1990) [56] and Falzarano (1990) [7]. In this case, the Melnikov function switches sign depending on the relative instantaneous position of the stable manifold with respect to the unstable manifold in the phase plane. The amount of phase space transported out of the safe region is related to the area of lobes formed where the unstable manifold lies outside the stable manifold. Since the Melnikov function is representative of the distance between the manifolds, the area of lobes where the unstable manifold lies outside of the stable manifold can be quantified in terms of the area under the Melnikov function when it is positive [12,17,20]. The rate at which solutions escape from the safe basin can then be calculated by taking a long term average of the positive part of the Melnikov function. This quantity is known as the rate of phase-space flux Φ and is defined mathematically as shown in (42) [34]

$$\Phi = \lim_{T\to\infty} \frac{1}{2T} \int_{-T}^{T} M^{+}(t_0)dt_0 \tag{42}$$

where $M^{+}(t_0)$ represents the positive part of the Melnikov function and is given by

$$M^{+}(t_0) = \begin{cases} M(t_0) & \text{if } M(t_0) \geq 0 \\ 0 & \text{otherwise} \end{cases} \tag{43}$$

Since $\tilde{M}(t_0)$ is an ergodic Gaussian process, it follows that the Melnikov process $M(t_0)$ is also an ergodic Gaussian process with a mean value of $\overline{M}$. Thus, the long term time average in (42) can be equated to an ensemble average as shown in (44).

$$\begin{aligned} \lim_{T\to\infty} \frac{1}{2T} \int_{-T}^{T} M^{+}(t_0)dt_0 &= E\left[M^{+}(t_0)\right] \\ &= E\left[(\overline{M} + \tilde{M}(t_0))^{+}\right] \end{aligned} \tag{44}$$

Using the probability density function for $\tilde{M}$ shown in (41), the rate of phase-space flux is given by

$$\begin{aligned} \Phi &= E\left[(\overline{M} + \tilde{M}(t_0))^{+}\right] \\ &= \int_{-\overline{M}}^{\infty} (x + \overline{M}) p_{\tilde{M}}(x) dx \\ &= \int_{-\overline{M}}^{\infty} (x + \overline{M}) \frac{1}{\sqrt{2\pi}\sigma_{\tilde{M}}} \exp\left(-\frac{x^2}{2\sigma_{\tilde{M}}^2}\right) dx \\ &= \sigma_{\tilde{M}} \int_{-\frac{\overline{M}}{\sigma_{\tilde{M}}}}^{\infty} (z + \frac{\overline{M}}{\sigma_{\tilde{M}}}) \frac{1}{\sqrt{2\pi}} \exp\left(-\frac{z^2}{2}\right) dz \\ &= \left[\sigma_{\tilde{M}} p\left(\frac{-\overline{M}}{\sigma_{\tilde{M}}}\right) + \overline{M}\left(1 - P\left(\frac{-\overline{M}}{\sigma_{\tilde{M}}}\right)\right)\right] \end{aligned} \tag{45}$$

where $p(.)$ and $P(.)$ represent the probability density function and cumulative probability distribution function of a standard normal distribution respectively.

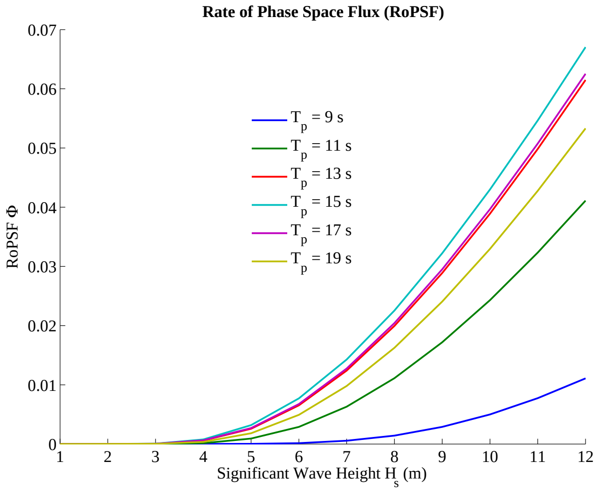

Fig. 12: Variation of rate of phase space flux with significant wave height H_s for various peak periods T_p

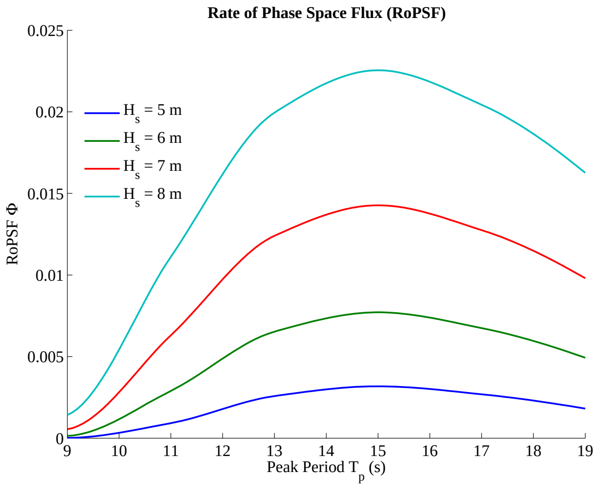

Fig. 13: Variation of rate of phase space flux with peak periods T_p for various significant wave heights H_s

The variation of the rate of phase space flux Φ with significant wave height for various peak periods is shown in Figure 12. The rate of phase space flux is non-zero for all non-zero wave heights, which means that the system has a finite probability of capsize as soon as the excitation is applied. However, the probability of capsize will be extremely low for small wave heights and will assume significant values only for larger wave heights.

The corresponding variation of the rate of phase space flux Φ with the peak period of the spectrum for various significant wave heights is shown in Figure 13.

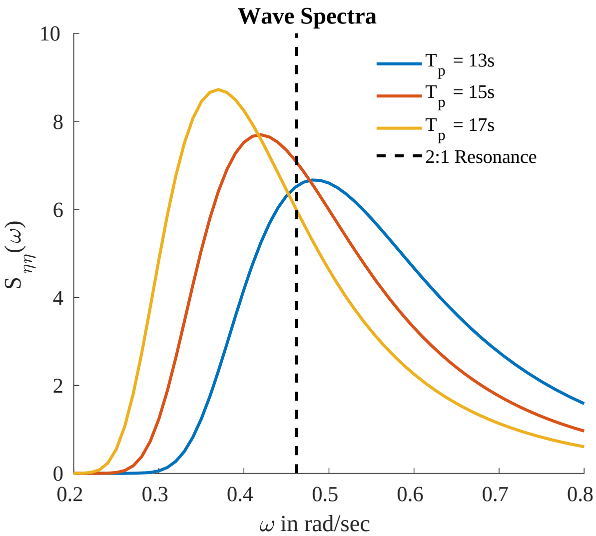

Fig. 14: Wave spectra with fixed significant wave height $H_s = 6\ m$ and varying peak period T_p at the $2:1$ subharmonic resonance frequency $0.462\ rad/s$

The rate of phase space flux increases with an increase in the peak period until $T_p \approx 15\ s$ and then decreases with a further increase in period.

This seems counterintuitive as peak of rate of phase flux does not coincide with the $2:1$ subharmonic resonant period of ($13.6\ s$) for the modified C11 hull form. However, this can be explained as follows. Consider the wave spectra with three peak periods ($T_p = 13\ s,\ 15\ s$ and $17\ s$) overlaid with the $2:1$ subharmonic resonance frequency ($\frac{2\pi}{13.6} = 0.4620\ rad/s$) as shown in Figure 14. It can be seen that at the $2:1$ subharmonic resonance frequency, the energy of the spectrum with peak period of $T_p = 15\ s$ is the higher than the energy of the other two spectra. Thus, it is expected that the spectrum with peak period of $T_p = 15\ s$ leads to more parametric excitation than the other two spectra and hence corresponds to the highest rate of phase space flux in Figure 13.

If $\sigma^{(1)}_{\tilde{M}}$ is denoted as the RMS value of the oscillatory part of Melnikov function when the system is excited by a unit significant wave height, the rate of phase space flux can be expressed as

$$\Phi = \left[\sigma^{(1)}_{\tilde{M}} H_s p \left(\frac{-\overline{M}}{\sigma^{(1)}_{\tilde{M}} H_s} \right) + \overline{M} \left(1 - P \left(\frac{-\overline{M}}{\sigma^{(1)}_{\tilde{M}} H_s} \right) \right) \right] \tag{46}$$

As the significant wave height is increased, the rate of phase space flux also increases steadily until it reaches a linear asymptote. This limiting behavior can also be derived mathematically from (46) by taking the limit $H_s \to \infty$. The rate of phase space flux approaches a linear asymptote given by (47).

$$\Phi = \left[\frac{1}{\sqrt{2\pi}} \sigma^{(1)}_{\tilde{M}} H_s + \frac{1}{2} \overline{M} \right] \tag{47}$$

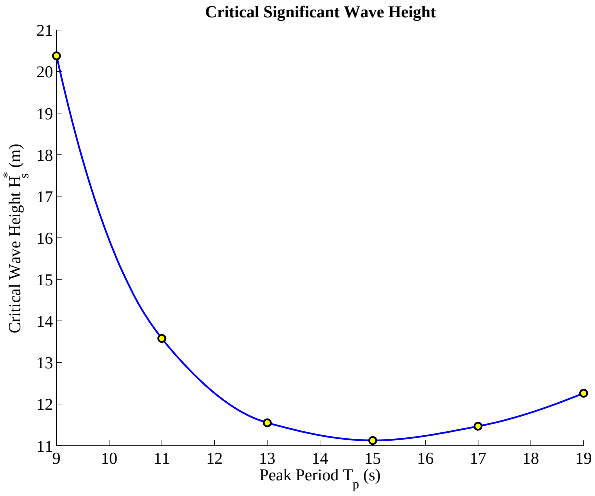

Fig. 15: Variation of critical significant wave height with peak period of spectrum

This linear asymptote has an intercept of H_s^* corresponding to zero phase space flux. This value is defined as the critical wave height and corresponds to the significant wave height at which substantial phase space flux is initiated. The mathematical expression for H_s^* is given by

$$H_s^* = -\sqrt{\frac{\pi}{2}} \frac{\overline{M}}{\sigma_{\tilde{M}}^{(1)}} \tag{48}$$

Since the rate of phase space flux increases almost linearly with significant wave height beyond $H_s = H_s^*$, the critical significant wave height H_s^* can be thought of as providing a limiting value of significant wave height H_s for a given peak period beyond which the vessel has a higher probability of capsizing. Although an exact mathematical dependence between critical significant wave height and the probability of capsize is unknown at present, there are several studies [17, 20, 21] that have demonstrated that the critical significant wave height H_s^* predicted using the Melnikov analysis does agree well with the estimated H_s boundary (calculated using Monte Carlo simulations) beyond which the capsize probability increases rapidly.

The variation of critical significant wave height with the peak period of the spectrum is shown in Figure 15. Due to the tuned nature of parametric excitation and observed variation of rate of phase space flux with peak period (Figure 13), the critical significant wave height is expected to be lowest when the peak period is close to the $2:1$ subharmonic resonance period. It is also expected to increase quickly as the peak period shifts away from the subharmonic resonance period. Figure 15 displays this expected behavior of the critical significant wave height.

However, if a designer deems the capsize probability corresponding to a critical significant wave height H_s^* to be either too high or too low, an alternate criterion can be used to estimate the limiting significant wave height based on the specified values of rate of phase space flux. In this case, the limiting value of H_s is obtained

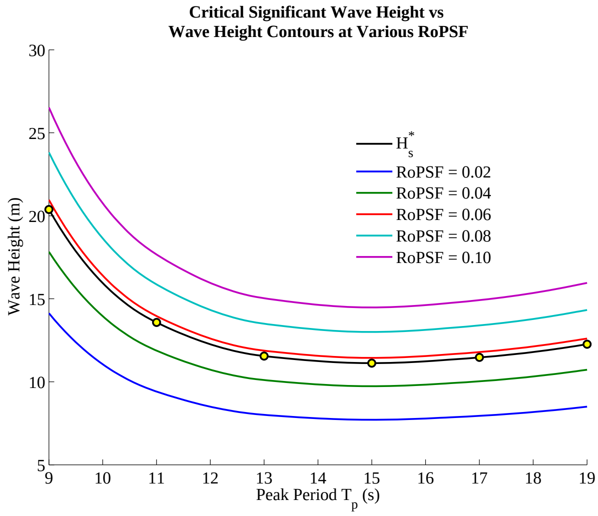

Fig. 16: Variation of critical significant wave height with peak period of spectrum

by solving (46) after setting the rate of phase space flux to a prescribed value chosen by the designer. A comparison of the limiting values of H_s using this approach for various specified values of rate of phase space flux and critical significant wave height H_s^* is shown in Figure 16. Although H_s^* seems to have a trend similar to the limiting H_s obtained by equating phase space flux to a constant value, it is important to remember that rate of phase space flux Φ is not constant as peak period varies along the H_s^* curve.

It can be seen from (46) and (48) that both rate of phase space flux Φ and critical significant wave height H_s^* depend on the mean value of Melnikov function $\overline{M}$ and the root mean square (RMS) value of the oscillatory component of Melnikov function when the system is excited by a unit significant wave height $\sigma_{\tilde{M}}^{(1)}$. While $\overline{M}$ depends on damping in the system, $\sigma_{\tilde{M}}^{(1)}$ is a function of input wave elevation. While the calculation of $\overline{M}$ and $\sigma_{\tilde{M}}^{(1)}$ are not based off of analytical expressions (due to the use of 11^{th} order stiffness instead of a 3^{rd} or 5^{th} order approximation with closed form expressions for $[x_0(t)\ y_0(t)]^T$), the computation involved is minuscule. Thus, rate of phase space flux Φ and critical significant wave height H_s^* can be effectively used as design criteria for assessment of stability of parametric response of a vessel in head seas.

9 Stochastic Averaging Approach

Simiu (2002) [34] compared the rate of phase space flux of a Duffing-Holmes oscillator with the mean first escape rate $\frac{1}{\tau_{FP}}$ (defined as the inverse of mean first passage time τ_{FP}) estimated from Monte Carlo simulations and demonstrated that the two quantities are proportional to each other. Based on this observed proportionality Simiu further suggested the possible use of the rate of phase space flux as a measure of escape rate. A similar comparison of the mean escape rate and the rate of phase space flux for directly excited roll motion was investigated by Su and Falzarano (2013) [51]. However, the difference in this study was that mean first passage time was estimated by applying stochastic averaging technique instead of using Monte Carlo simulations.

The stochastic averaging technique approximates the energy of the system as a Markov process. The Markov approximation of energy allows for the complicated first passage problem of the original system to be simplified into a boundary value problem that is known as the Pontryagin equation. The solution of this boundary value problem yields the mean first passage time of the system. Similar to rate of phase space flux calculation, this approach too requires only a small computational effort and provides a relatively quick approach to compare several interim designs. In this study, the stochastic averaging approach is adopted to compute mean first passage times of the system instead of performing time consuming Monte Carlo simulations.

This section provides a brief overview of the stochastic averaging approach for completeness. For more details the readers are referred to Somayajula et al. (2019) [40]. A comparison between the rate of phase space flux and the mean first escape rate (computed from the mean first passage times) is discussed in section 10.

The roll equation of motion can be expressed as

$$\begin{aligned}\ddot{x} + \epsilon^2\delta_{1\epsilon}\dot{x} + \epsilon^2\delta_{2\epsilon}\dot{x}|\dot{x}| + \Big[x + \alpha_3 x^3 + \alpha_5 x^5 + ...\Big] \\ + \Big[\epsilon p_1(t)x + \epsilon p_3(t)x^3 + \epsilon p_5(t)x^5 + ...\Big] = 0 \end{aligned} \tag{49}$$

where $\delta_{1\epsilon} = \frac{\delta_1}{\epsilon}$ and $\delta_{2\epsilon} = \frac{\delta_2}{\epsilon}$. This rescaling of the damping is performed to ensure that mathematically the standard deviation of the response is $O(\epsilon)$ as $\epsilon \to 0$ and does not imply that excitation is weak [32]. The rate of change of energy of the system can be found by differentiating (16) with respect to time and is given by

$$\begin{aligned}\dot{E} &= \dot{x}\Big[\ddot{x} + x + \alpha_3 x^3 + \alpha_5 x^5 + ...\Big] \\ &= -\epsilon^2\Big[\delta_{1\epsilon}\dot{x}^2 + \delta_{2\epsilon}\dot{x}^2|\dot{x}|\Big] - \epsilon\dot{x}\Big[p_1(t)x + p_3(t)x^3 + p_5(t)x^5 + ...\Big]\end{aligned} \tag{50}$$

It can be seen from (50) that the energy of the system varies slowly, which allows it to be approximated as a Markov process [40] governed by the stochastic differential equation shown below

$$dE = m_1(E)dt + \sigma_{11}(E)dB_t \tag{51}$$

where B_t represents Brownian motion process, $m_1(E)$ and $\sigma_{11}(E)$ are called the drift and diffusion coefficients respectively and are determined using the parameters in (49). Expressions for the drift and diffusion coefficients are given by

$$
\begin{aligned}
m_1(E) =& A_1(E) + \sum_{j=1,3,5,\ldots}^{N_q} \sum_{k=1,3,5,\ldots}^{N_q} \left[\left(\int_{-\infty}^{0} R_{jk}(\tau) d\tau \right) \left\{ a_0^{(1j)} a_0^{(1k)} + a_0^{(2j)} a_0^{(1k)} \right\} \right. \\
& + \sum_{n=1}^{\infty} \left(\int_{-\infty}^{0} R_{jk}(\tau) \cos\left(\frac{2\pi n}{T(E)} \tau \right) d\tau \right) \\
& \left. \times \left\{ \frac{b_n^{(1j)} b_n^{(1k)}}{2} + \frac{a_n^{(1j)} a_n^{(1k)}}{2} + (j) \frac{b_n^{(2j)} b_n^{(1k)}}{2} + (j) \frac{a_n^{(2j)} a_n^{(1k)}}{2} \right\} \right]
\end{aligned} \tag{52}
$$

$$
\begin{aligned}
D_{11}(E) &= \sigma_{11}^2(E) \\
&= \sum_{n=1}^{\infty} \sum_{j=1,3,5,\ldots}^{N_q} \sum_{k=1,3,5,\ldots}^{N_q} \left[(2\pi E) \left\{ b_n^{(1j)} b_n^{(1k)} \right\} S_{jk}^{(c)} \left(\frac{2\pi n}{T(E)} \right) \right]
\end{aligned} \tag{53}
$$

where $a_n^{(1k)}$, $b_n^{(1k)}$, $a_n^{(2k)}$ and $b_n^{(2k)}$ are Fourier series coefficients and satisfy the following equations:

$$\sin(\theta_0(t)) x_0^k(t) = \sum_{n=1}^{\infty} b_n^{(1k)} \sin\left(\frac{2\pi n}{T(E)} t \right) \tag{54}$$

$$\cos(\theta_0(t)) x_0^k(t) = a_0^{(1k)} + \sum_{n=1}^{\infty} a_n^{(1k)} \cos\left(\frac{2\pi n}{T(E)} t \right) \tag{55}$$

$$\frac{2E \sin(\theta_0(t)) \cos^2(\theta_0(t)) x_0^{k-1}(t)}{g(E, \theta_0(t))} = \sum_{n=1}^{\infty} b_n^{(2k)} \sin\left(\frac{2\pi n}{T(E)} t \right) \tag{56}$$

$$\frac{2E \sin^2(\theta_0(t)) \cos(\theta_0(t)) x_0^{k-1}(t)}{g(E, \theta_0(t))} = a_0^{(2k)} + \sum_{n=1}^{\infty} a_n^{(2k)} \cos\left(\frac{2\pi n}{T(E)} t \right) \tag{57}$$

where $\theta_0(t) = \tan^{-1}\left[-\frac{\dot{x}_0(t)}{\sqrt{2U(x_0(t))}} \right]$, $x_0(t)$ and $\dot{x}_0(t)$ are phase, displacement and velocity of the unperturbed system ($\epsilon = 0$) respectively for a specified energy E. Additionally, $g(E, \theta_0(t)) = x_0(t) + \sum_{i=3,5,..}^{N_q} \alpha_i x_0^i(t)$. Cosine and sine cross spectra $S_{jk}^{(c)}(\Omega)$ and $S_{jk}^{(s)}(\Omega)$ are defined as

$$S_{jk}^{(c)}(\Omega) = \frac{1}{2\pi} \int_{-\infty}^{\infty} R_{jk}(\tau) \cos(\Omega \tau)\, d\tau \tag{58}$$

$$S_{jk}^{(s)}(\Omega) = \frac{1}{2\pi} \int_{-\infty}^{\infty} R_{jk}(\tau) \sin(\Omega \tau)\, d\tau \tag{59}$$

where $R_{jk}(\tau) = E\left[p_j(t) p_k(t+\tau) \right]$. Coefficient $A_1(E)$ in (52) is calculated as

$$A_1(E) = -\frac{1}{T(E)} \int_0^{T(E)} \left(\delta_{1\epsilon} \dot{x}_0^2(t) + \delta_{2\epsilon} \dot{x}_0^2(t) |\dot{x}_0(t)| \right) dt \tag{60}$$

Figure 17 and Figure 18 show the variation of the drift and diffusion coefficients with significant wave height and peak wave period respectively. It can be seen

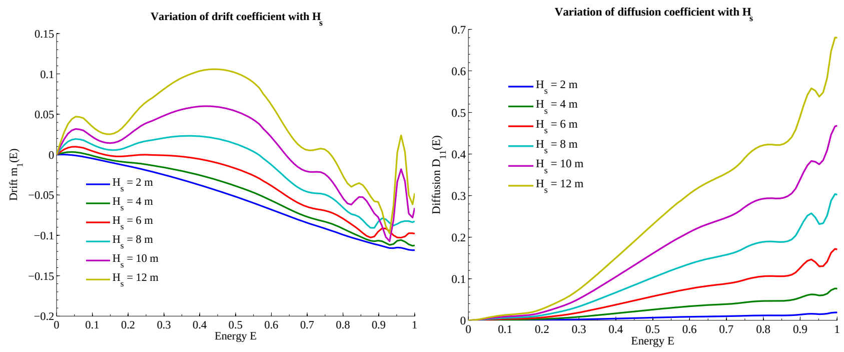

(a) Drift coefficient $m_1(E)$ (b) Diffusion coefficient $D_{11}(E)$

Fig. 17: Variation of drift and diffusion coefficients with significant wave height $H_s =$ for a fixed peak period $T_p = 13$ *sec*

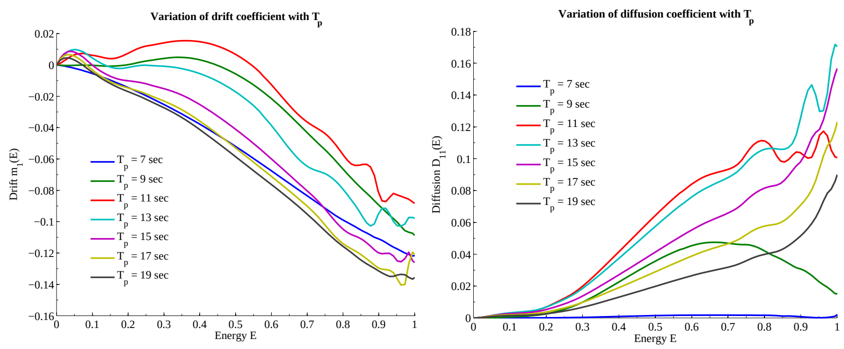

(a) Drift coefficient $m_1(E)$ (b) Diffusion coefficient $D_{11}(E)$

Fig. 18: Variation of drift and diffusion coefficients with peak period T_p for a fixed significant wave height $H_s = 6\ m$

that the drift and diffusion coefficients increase monotonically with an increase in significant wave height. However, both the drift and diffusion coefficients increase with an increase in peak period up to $T_p = 13$ *sec* and then decrease with a further increase in the peak period. Thus as the encounter frequency of peak period of the spectrum comes close to $2\omega_n$, the system exhibits stronger drift and diffusion coefficients. This is consistent with the well known tuned behavior ($\omega_e : \omega_n = 2 : 1$) of subharmonic parametric resonance.

The first passage time τ_{FP} of the system is defined as the random time when energy process $E(t)$ reaches a critical value E_c for the first time given that the system starts from an initial energy level E_0 at $t = 0$. Since $E(t)$ is a Markov process, moments of the first passage time are governed by a recursive set of differential equations known as Pontryagin equations. Corresponding differential equation governing the mean of first passage time $\mu_1(E_0) = E[\tau_{FP}]$ for the system starting with an initial energy E_0 is given by

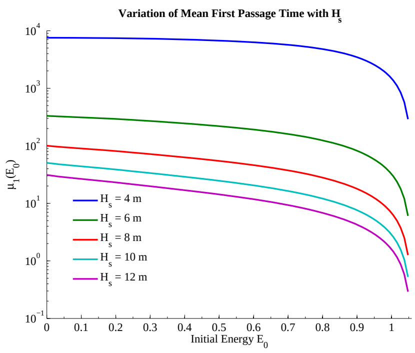

(a) Fixed $T_p = 13\ sec$

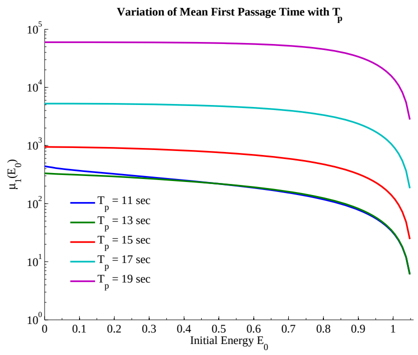

(b) Fixed $H_s = 6\ m$

Fig. 19: Variation of mean first passage time with significant wave height H_s and peak period T_p

$$1 + m_1(E_0)\frac{d\mu_1}{dE_0} + \frac{1}{2}D_{11}(E_0)\frac{d^2\mu_1}{dE_0^2} = 0 \tag{61}$$

The boundary conditions for (61) are given by

$$\mu_1(E_c) = 0 \tag{62}$$

$$E_0\frac{d\mu_1}{dE_0}(E_0) = \frac{-2}{\pi S_{11}^c(2) - 2\delta_{1\epsilon}} \text{ as } E_0 \to 0 \tag{63}$$

The second boundary condition is obtained by linearizing the system close to the boundary $E_0 = 0$. Only the linear stiffness and linear damping are retained in the linearized system due to the contribution from nonlinearities being negligible near $E_0 = 0$. Application of stochastic averaging to this linearized system results in the boundary condition given by (63). Mathematical details on the derivation of the boundary condition can be found in the appendix of Somayajula et al (2019) [40].

This boundary value problem can be solved numerically to calculate the mean first passage time. The variation of the mean first passage times with varying significant wave heights and peak periods are shown in Figure 19a and Figure 19b respectively. The Pontryagin equation is not applicable for $T_p = 7\ sec$ and $T_p = 9\ sec$ as the system does not exhibit a parametric resonance and hence these cases are not shown in Figure 19b. An increase in significant wave height results in a decrease in mean first passage time. The mean first passage time is lowest for $T_p = 13\ sec$ and increases as peak period is further increased. This is consistent with the tuned behavior of parametric resonance. In this study, the mean first passage time for the system starting with zero initial energy $\mu_1(0)$ is used as an independent metric to quantify the stability of a system.

10 Comparison of Markov and Melnikov Approaches

In the previous sections, the Melnikov and Markov approaches to assess stability of a vessel vulnerable to parametric roll in irregular head seas have been described. In Melnikov approach, the rate of phase space flux is used as the metric to quantify stability. Correspondingly the stability metric in the stochastic averaging technique is the mean first passage time.

In this section the sensitivity of the stability metrics from both approaches are compared for various cases. The sensitivity study is performed by comparing the stability metrics from both methods for a range of cases where the following two parameters are varied:

- Significant wave height H_s
- Peak period T_p

Figure 20a shows the variation of the rate of phase space flux and mean first escape rate (defined as the inverse of the mean first passage time) with significant wave height. It can be seen that both the mean first escape rate $\frac{1}{\mu_1(0)}$ and rate of phase space flux Φ vary monotonically with H_s although the rate of phase space flux is almost twice the mean first escape rate calculated by stochastic averaging. The plot of the rate of phase space flux against mean first escape rate shown in Figure 20b demonstrates that the two quantities are linearly related. This suggests that using either metric for analysis will lead to the same conclusion when comparing one design relative to another.

Figure 21 shows the variation of the rate of phase space flux and mean first escape rate with the peak period of spectrum. Although both the rate of phase space flux and mean first escape rate demonstrate similar trends of initially increasing and eventually decreasing with an increase in peak period, their sensitivity seems to differ. While the mean first escape rates peak at $T_p = 13$ *sec*, rate of phase space fluxes peak at $T_p = 15$ *sec*. Thus although the two metrics have similar trends in variation with T_p, their sensitivity to peak period T_p is different.

11 Lyapunov Exponent

In this study, the Melnikov function is used to calculate the rate of phase space flux. However, it is well known from the theory of chaotic dynamics that a positive Melnikov function is also a necessary condition for a system to demonstrate chaos [22]. It is evident from the results shown above that the Melnikov function does attain positive values, which leads to an increase of the rate of phase space flux. To determine whether the response observed is chaotic or not, we investigate the Lyapunov exponents of the system.

It is known from the theory of chaotic dynamics [4] that one of the necessary conditions for a system to exhibit chaotic response is its sensitive dependence to initial conditions. Sensitive dependence on initial conditions means that two orbits arbitrarily close to each other in the phase space at a particular time will eventually diverge from each other at an exponential rate. One of the ways to ascertain whether a system possesses sensitive dependence to initial conditions is to evaluate Lyapunov exponents of the system. Lyapunov exponents are defined

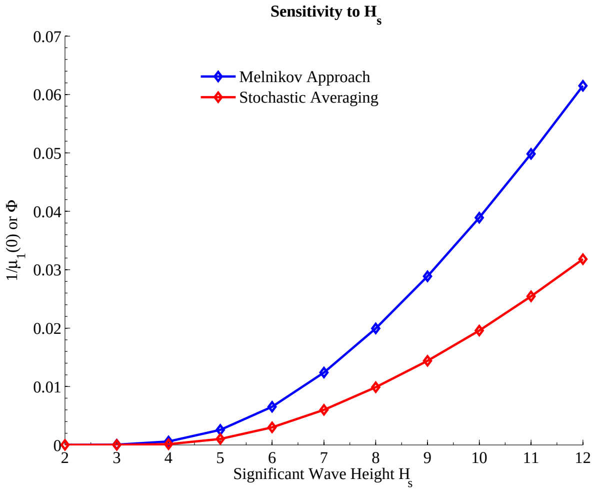

(a) Sensitivity ($T_p = 13.0\ s$)

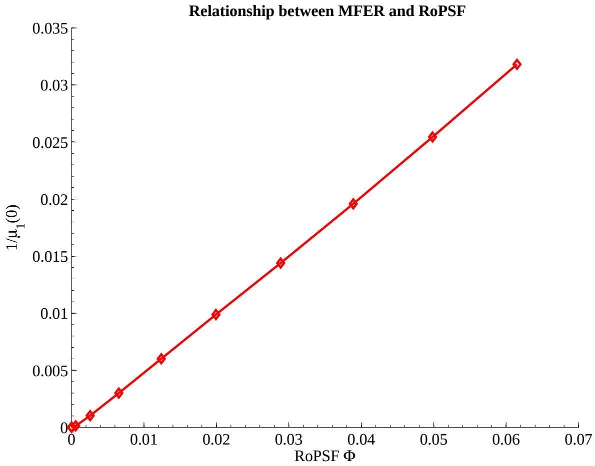

(b) Relationship for $T_p = 13.0\ s$ (Slope: 0.52)

Fig. 20: Comparison of mean first escape rate and rate of phase space flux

as the average exponential rates of convergence or divergence of nearby orbits in the phase plane [58].

Therefore, it is clear that for a motion converging to a fixed point, like a node, all the Lyapunov exponents must be negative. Similarly, for a periodic motion at least one Lyapunov exponent must be zero and finally for chaotic motion, at least one Lyapunov exponent must be positive. While the sign of the Lyapunov exponent ascertains if a system is chaotic or not, its value quantifies the chaos in a system. For certain simple systems it is possible to evaluate the largest Lyapunov exponent analytically. However, for most real world examples this is not possible. When an analytical expression cannot be derived, the exponent is estimated numerically

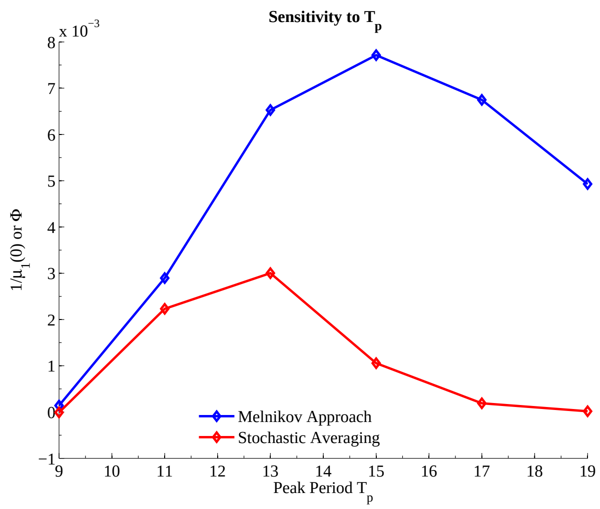

Fig. 21: Sensitivity of mean first escape rate and rate of phase space flux to peak period ($H_s = 6.0\ m$)

from a time history of the process obtained either from experiments or simulations. One such algorithm to calculate the largest Lyapunov exponent from a simulated or experimentally measured time history has been developed by Wolf et al. (1985) [58]. This algorithm encoded as a MATLAB program is also freely available on the web and has been utilized in evaluating the largest Lyapunov exponent from simulated roll motion time series data in this study. The approach of Lyapunov exponents to harmonically forced ship roll motion was previously discussed by Falzarano (1990) [7].

While calculating the largest Lyapunov exponent from time series data is fairly accurate, an approximate estimate of Lyapunov exponent in the vicinity of the stable equilibrium point can also be obtained in analytical form using the stochastically averaged system described in section 9 [59]. Consider a n-dimensional stochastic process $\boldsymbol{X}(t)$ whose stability is of interest. Let $||\boldsymbol{X}(t)||$ denote the Euclidean norm of the vector $\boldsymbol{X}(t)$ defined by (64).

$$||\boldsymbol{X}(t)|| = \sqrt{\boldsymbol{X}^T(t)\boldsymbol{X}(t)} = \sqrt{\left[\sum_{i=1}^{n} X_i^2(t)\right]} \tag{64}$$

Then Lyapunov exponent λ is defined as the average exponential rate of convergence or divergence of the norm and can mathematically be written as shown in (65).

$$\lambda = \lim_{t\to\infty} \frac{1}{t} \ln(||\boldsymbol{X}(t)||) \tag{65}$$

For a one dimensional system $V(t)$ this expression reduces to (66).

$$\lambda = \lim_{t\to\infty} \frac{1}{t} \ln(V(t)) \tag{66}$$

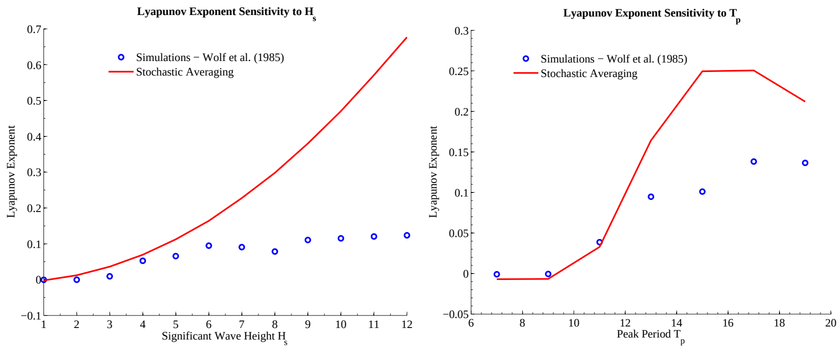

(a) Fixed $T_p = 13\ sec$ (b) Fixed $H_s = 6\ m$

Fig. 22: Variation of Lyapunov exponents with significant wave height H_s and peak period T_p

From section 9 we know that the energy E in the roll system can be approximated as a one dimensional Markov process and is governed by the Itô SDE shown in (51). Linearizing this system about the equilibrium point $E = 0$, the SDE governing the dynamics in the vicinity of the trivial solution $E = 0$ can be expressed as

$$dE = m_1'(0)Edt + \sigma_{11}'(0)EdB_t \tag{67}$$

where $m_1'(E)$ and $\sigma_{11}'(E)$ represent the derivative of the drift $m_1(E)$ and diffusion $\sigma_{11}(E)$ coefficients with respect to E. The Itô equation governing $\ln(E(t))$ can be obtained by applying the Itô formula and is given by

$$d(\ln(E)) = \left\{ m_1'(0) - \frac{1}{2}\left[\sigma_{11}'(0)\right]^2 \right\} dt + \sigma_{11}'(0)dB_t \tag{68}$$

Solution of this SDE is given by

$$\ln(E) = \ln(E_0) + \int_0^t \left\{ m_1'(0) - \frac{1}{2}\left[\sigma_{11}'(0)\right]^2 \right\} dt + \int_0^t \sigma_{11}'(0)dB_t \tag{69}$$

Now, Lyapunov exponent near the trivial solution $E = 0$ can be obtained by applying the definition shown in (66) and is given by

$$\begin{aligned} \lambda &= \lim_{t\to\infty} \frac{1}{t}\ln(E) \\ &= \lim_{t\to\infty} \frac{1}{t}\int_0^t \left\{ m_1'(0) - \frac{1}{2}\left[\sigma_{11}'(0)\right]^2 \right\} dt \\ &= \left\{ m_1'(0) - \frac{1}{2}\left[\sigma_{11}'(0)\right]^2 \right\} \end{aligned} \tag{70}$$

A comparison of the Lyapunov exponents calculated from simulated time histories and the stochastic averaging approach for increasing significant wave heights are shown in Figure 22a. Simulations show that although for smaller values of H_s, Lyapunov exponents increase monotonically with significant wave height, at larger values of H_s the exponents saturate to values much less than unity. This indicates that the response of the system does indicate some sensitivity to initial conditions. However, the value of the Lyapunov exponent is significantly close to zero suggesting that the response is fairly periodic. This means that the stochastic nature of the response is only due to the stochastic nature of the excitation and the system does not exhibit any chaotic behaviour.

At smaller significant wave heights, the excitation is fairly low and the subharmonic response is close to $E = 0$. However, as significant wave height increases, the system exhibits a strong parametric response that is no longer close to $E = 0$. This leads to a divergence between the Lyapunov exponents predicted from simulations and those obtained from stochastic averaging. Since the estimate from stochastic averaging is an approximation of the largest Lyapunov exponent at $E = 0$, it is only representative of the local behavior and is not as accurate as the value calculated from time series.

Figure 22b shows the variation of the Lyapunov exponents with peak period. At lower peak periods $T_p \leq 9$ *sec*, the system does not demonstrate any parametric response as the excitation signal does not have sufficient energy at frequencies close to $2\omega_n$. The exponents for these peak periods are slightly less than zero as the response signal consists of the decay of initial condition with time. As the peak period increases, the energy in the spectrum around $2\omega_n$ increases and Lyapunov exponents are found to settle to values slightly higher than zero but still not significantly far from zero.

12 Conclusion

In this paper a new approach to effectively estimate the vulnerability of a vessel to parametric roll in irregular seas is developed. A previously developed analytical model (Volterra $\overline{GZ}$ method) for parametric roll of a ship in a random seaway is analyzed using the Melnikov approach. Stability of the system is quantified in terms of rate of phase space flux Φ across the safe basin boundary and also in terms of critical significant wave height H_s^* beyond which significant increase in phase space flux is observed.

Designers can use the critical significant wave height H_s^* as a quick check to compare vulnerability of multiple designs. If the designer deems the H_s^* criterion to be too conservative, then a specified value of rate of phase space flux can be used as metric to compare interim designs. As both these criteria are evaluated using only the $1st$ order Volterra $\overline{GZ}$ transfer function, they can be analytically computed to help designer quickly compare vulnerability of the several designs to parametric excitation.

A brief description of an alternate method of stability analysis based on stochastic averaging approach is provided. In this method, the energy of the response is approximated as a Markov process and stability is quantified in terms of mean first passage time for the system to cross a certain threshold energy level. Sensitivity of stability metrics from both approaches to significant wave height and peak period are compared. While trends of both metrics are found to be in agreement for all the parameters studied, the stochastic averaging approach is found to be more sensitive to the peak period of excitation.

Finally, Lyapunov exponents of the system are analyzed. It is found that Lyapunov exponents of the system are positive but are very close to zero. It is concluded that for this specific example, the response in irregular waves does not exhibit any chaotic dynamics and is purely due to the subharmonic resonance of the system.

The critical significant wave height H_s^* and the rate of phase space flux Φ can be computed quickly due to the analytical nature of the method and are ideal for determining vulnerability of a design to parametric excitation. This method provides an effective estimate of the stability of a vessel subjected to parametric excitation without the need for simulating long time histories of the response. It is an ideal tool for a ship designer to quickly analyze and compare several interim hullform designs during basic design phase. In addition to having a strong foundation in the theory of nonlinear dynamical systems, this method is also practically relevant and in line with the second generation level 2 criteria being discussed by the International Maritime Organization (IMO).

Acknowledgments: The authors would like to thank Dr. Frans van Walree of MARIN for making available to us the modified C11 hull form description for our analysis. The authors would also like to thank Dr. Loren Lutes, emeritus professor with the department of Civil Engineering at Texas A&M University, for his guidance in developing the Markov approach. Finally, the authors would like to thank Dr. Paul Hess for facilitating the funding from Office of Naval Research (ONR).

Funding: The research described in this paper was supported by the Office of Naval Research (ONR) - ONR Grant N00014-16-1-2281.

Conflict of Interest: The authors declare that they have no conflict of interest.

References

1. Bulian, G.: Development of analytical nonlinear models for parametric roll and hydrostatic restoring variations in regular and irregular waves. Phd dissertation, Università degli studi di Trieste, Trieste (2006). URL `https://www.openstarts.units.it/dspace/handle/10077/2518`
2. Carmel, S.: Study of Parametric Rolling Event on a Panamax Container Vessel. Transportation Research Record: Journal of the Transportation Research Board **1963**, 56–63 (2006). DOI 10.3141/1963-08. URL `http://trrjournalonline.trb.org/doi/10.3141/1963-08`
3. Chai, W., Naess, A., Leira, B.J., Carlo, M.: Stochastic dynamic analysis and reliability of a vessel rolling in random beam seas. Journal of Ship Research **59**(2), 113–131 (2015). DOI 10.5957/JOSR.59.2.140059. URL `http://www.ingentaselect.com/rpsv/cgi-bin/cgi?ini=xref{&}body=linker{&}reqdoi=10.5957/JOSR.59.2.140059`
4. Devaney, R.: An Introduction to Chaotic Dynamical Systems, 1st edn. Addison Wesley Publishing Company, Redwood City (1989)
5. Esparza, I., Falzarano, J.: Nonlinear rolling motion of a statically biased ship under the effect of external and parametric excitation. In: S.C. Sinha, R.M. Evan-Iwanowski (eds.) Proceedings of the 14th Biennial Conference on Mechanical Vibration and Noise: Dynamics and Vibration of Time-Varying Systems and Structures, vol. 56, pp. 111–122. ASME, Albuquerque, NM (1993)
6. Falzarano, J., Somayajula, A., Seah, R.: An overview of the prediction methods for roll damping of ships. Ocean Systems Engineering **5**(2), 55–76 (2015). DOI 10.12989/ose.2015.5.2.055. URL `http://koreascience.or.kr/journal/view.jsp?kj=`

TPTPKZ{&}py=2015{&}vnc=v5n2{&}sp=55http://koreascience.or.kr/journal/view.jsp?kj=TPTPKZ{%}7B{&}{%}7Dpy=2015{%}7B{&}{%}7Dvnc=v5n2{%}7B{&}{%}7Dsp=55
7. Falzarano, J.M.: Predicting complicated dynamics leading to vessel capsizing. Phd dissertation, University of Michigan, Ann Arbor (1990). URL http://deepblue.lib.umich.edu/handle/2027.42/91674
8. Falzarano, J.M., Holappa, K., Taz-Ul-Mulk, M.: A generalized analysis of saturation induced ship rolling motion. In: J.M. Falzarano, F. Papoulias (eds.) Proceedings of the 1993 ASME Winter Annual Meeting: Nonlinear Dynamics of Marine Vehicles, vol. 51, pp. 73–92. ASME, New Orleans, LA (1993)
9. Falzarano, J.M., Shaw, S.W., Troesch, A.W.: Application of global methods for analyzing dynamical systems to ship rolling motion and capsizing. International Journal of Bifurcation and Chaos **2**(1), 101–115 (1992). DOI 10.1142/S0218127492000100. URL http://www.worldscientific.com/doi/abs/10.1142/S0218127492000100
10. Falzarano, J.M., Su, Z., Jamnongpipatkul, A., Somayajula, A.: Solving the Problem of Nonlinear Ship Roll Motion Using Stochastic Dynamics, pp. 423–435. Springer International Publishing, Cham (2019). DOI 10.1007/978-3-030-00516-0_25. URL https://doi.org/10.1007/978-3-030-00516-0{_}25
11. France, W., Levadou, M., Treakle, T.W., Paulling, J.R., Michel, R.K., Moore, C.: An investigation of head-sea parametric rolling and its influence on container lashing systems. Marine Technology **40**(1), 1–19 (2003). URL http://www.ingentaconnect.com/content/sname/mt/2003/00000040/00000001/art00001
12. Frey, M., Simiu, E.: Noise-induced chaos and phase space flux. Physica D: Nonlinear Phenomena **63**, 321–340 (1993). DOI 10.1016/0167-2789(93)90114-G
13. Froude, W.: On the rolling of ships (1861). URL http://scholar.google.com/scholar?q=on+the+rolling+of+ships+froude{&}btnG={&}hl=en{&}as{_}sdt=0{%}2C44{#}0
14. Greenspan, B., Holmes, P.: Repeated resonance and homoclinic bifurcation in a periodically forced family of oscillators. SIAM Journal on Mathematical Analysis **15**(1), 69–97 (1984). DOI 10.1137/0515003. URL http://epubs.siam.org/doi/10.1137/0515003
15. Guckenheimer, J., Holmes, P.: Nonlinear Oscillations, Dynamical Systems, and Bifurcations of Vector Fields, *Applied Mathematical Sciences*, vol. 42, 1st edn. Springer New York, New York (1983). DOI 10.1007/978-1-4612-1140-2. URL http://appliedmechanics.asmedigitalcollection.asme.org/article.aspx?articleid=1407863http://link.springer.com/10.1007/978-1-4612-1140-2
16. Hsieh, S.R., Shaw, S.W., Troesch, A.W.: A predictive method for vessel capsize in random seas. In: J.M. Falzarano, F. Papoulias (eds.) Proceedings of the 1993 ASME Winter Annual Meeting: Nonlinear Dynamics of Marine Vehicles, vol. 51, pp. 103–123. ASME, New Orleans, LA (1993)
17. Hsieh, S.R., Troesch, A.W., Shaw, S.W.: A nonlinear probabilistic method for predicting vessel capsizing in random beam seas. Proceedings of the Royal Society A: Mathematical, Physical and Engineering Sciences **446**(1926), 195–211 (1994). DOI 10.1098/rspa.1994.0099. URL http://rspa.royalsocietypublishing.org/cgi/doi/10.1098/rspa.1994.0099
18. Huang, X., Gu, X., Bao, W.: The probability distribution of rolling amplitude of a ship in high waves. In: Proceedings of 5th International Conference on Stability of Shipsand Oean Vehicles (STAB94), vol. 4, pp. 77–100. STAB International Standing Committee, Melbourne, FL (1994)
19. Ikeda, Y., Himeno, Y., Tanka, N.: A Prediction Method for Ship Roll Damping. Tech. rep., University of Osaka Prefecture, Osaka, Japan (1978). DOI Reportno00405. URL http://www.marine.osakafu-u.ac.jp/{~}lab15/papersearch/papers/PDF/A23.pdf
20. Jiang, C.: Highly nonlinear rolling motion leading to capsize. Phd dissertation, University of Michigan, Ann Arbor (1995)
21. Jiang, C., Troesch, A.W., Shaw, S.W.: Capsize criteria for ship models with memory-dependent hydrodynamics and random excitation. Philosophical Transactions of the Royal Society A: Mathematical, Physical and Engineering Sciences **358**(1771), 1761–1791 (2000). DOI 10.1098/rsta.2000.0614. URL http://rsta.royalsocietypublishing.org/cgi/doi/10.1098/rsta.2000.0614http://rsta.royalsocietypublishing.org/content/358/1771/1761.shorthttp://rsta.royalsocietypublishing.org/content/358/1771/1761
22. Jordan, D.W., Smith, P.: Nonlinear Ordinary Differential Equations : An Introduction to Dynamical Systems, 4th edn. Oxford University Press, New York (1999)
23. Lou, J., Xie, G.: Solution methods of complex nonlinear dynamic systems in offshore engineering. Tech. rep., Offshore Technology Research Center, Texas A&M University, College Station, TX, USA (1993)

24. Melnikov, V.: On the stability of the center for time-periodic perturbations. Transactions of Moscow Mathematical Society **12**, 1–57 (1963). URL https://scholar.google.com/scholar?hl=en{&}q=+On+the+stability+of+the+center+for+time+periodic+perturbations{&}btnG={&}as{_}sdt=1{%}2C44{&}as{_}sdtp={#}0
25. Moideen, H., Falzarano, J.M., Sharma, S.: Parametric roll of container ships in head waves. Ocean Systems Engineering **2**(4), 239–255 (2012). DOI 10.12989/ose.2012.2.4.239. URL http://koreascience.or.kr/journal/view.jsp?kj=TPTPKZ{%}7B{&}{%}7Dpy=2012{%}7B{&}{%}7Dvnc=v2n4{%}7B{&}{%}7Dsp=239http://koreascience.or.kr/journal/view.jsp?kj=TPTPKZ{&}py=2012{&}vnc=v2n4{&}sp=239
26. Moideen, H., Somayajula, A., Falzarano, J.M.: Parametric Roll of High Speed Ships in Regular Waves. In: Volume 5: Ocean Engineering, p. V005T06A095. ASME, Nantes, France (2013). DOI 10.1115/OMAE2013-11602. URL http://proceedings.asmedigitalcollection.asme.org/proceeding.aspx?articleid=1786500http://proceedings.asmedigitalcollection.asme.org/proceeding.aspx?doi=10.1115/OMAE2013-11602
27. Moideen, H., Somayajula, A., Falzarano, J.M.: Application of Volterra series analysis for parametric rolling in irregular seas. Journal of Ship Research **58**(2), 97–105 (2014). DOI 10.5957/JOSR.58.2.130047. URL http://www.ingentaconnect.com/content/sname/jsr/pre-prints/content-JOSR130047
28. Moseley, H.: On the dynamical stability and on the oscillations of floating bodies. Philosophical Transactions of the Royal Society of London **140**, 609–643 (1850). URL http://www.jstor.org/stable/108454
29. Nayfeh, A.H., Khdeir, A.A.: Nonlinear rolling of ships in regular beam seas. International Shipbuilding Progress **33**(379), 40–49 (1986). URL http://cat.inist.fr/?aModele=afficheN{&}cpsidt=8610233
30. Parker, T.S., Chua, L.O.: Practical Numerical Algorithms for Chaotic Systems, 1st edn. Springer, New York (1989). DOI 10.1007/978-1-4612-3486-9. URL http://link.springer.com/10.1007/978-1-4612-3486-9
31. Roberts, J.: Nonlinear Analysis of Slow Drift Oscillations of Moored Vessels in Random Seas. Journal of Ship Research **25**(2), 130–140 (1981)
32. Roberts, J.B., Vasta, M.: Energy-based stochastic estimation for nonlinear oscillators with random excitation. Journal of Applied Mechanics **67**(4), 763–771 (2000). DOI 10.1115/1.1330546. URL http://cat.inist.fr/?aModele=afficheN{&}cpsidt=908977http://appliedmechanics.asmedigitalcollection.asme.org/article.aspx?articleid=1414121
33. Scolan, Y.M.: Application de la méthode de Melnikov pour l'étude du roulis non linéaire des navires dans la houle. Comptes Rendus de l'Académie des Sciences - Series IIB - Mechanics-Physics-Astronomy **327**(1), 1–6 (1999). DOI 10.1016/S1287-4620(99)80002-7. URL http://linkinghub.elsevier.com/retrieve/pii/S1287462099800027
34. Simiu, E.: Chaotic Transitions in Deterministic and Stochastic Dynamical Systems: Applications of Melnikov Processes in Engineering, Physics, and Neuroscience, 1st edn. Princeton University Press, New Jersey (2002)
35. Somayajula, A., Falzarano, J.: Large-amplitude time-domain simulation tool for marine and offshore motion prediction. Marine Systems & Ocean Technology **10**(1), 1–17 (2015). DOI 10.1007/s40868-015-0002-7. URL http://link.springer.com/10.1007/s40868-015-0002-7
36. Somayajula, A., Falzarano, J.: Estimation of roll motion parameters using R-MISO system identification technique. In: J.S. Chung, M. Muskulus, T. Kokkinis, A.M. Wang (eds.) 26th International Offshore and Polar Engineering (ISOPE 2016) Conference, vol. 3, pp. 568–574. International Society of Offshore and Polar Engineers (ISOPE), Rhodes (Rodos), Greece (2016)
37. Somayajula, A., Falzarano, J.: Application of advanced system identification technique to extract roll damping from model tests in order to accurately predict roll motions. Applied Ocean Research **67**, 125–135 (2017). DOI 10.1016/j.apor.2017.07.007. URL http://linkinghub.elsevier.com/retrieve/pii/S0141118717302316
38. Somayajula, A., Falzarano, J.: Critical assessment of reverse-MISO techniques for system identification of coupled roll motion of ships. Journal of Marine Science and Technology **22**(2), 231–244 (2017). DOI 10.1007/s00773-016-0406-x. URL http://link.springer.com/10.1007/s00773-016-0406-x
39. Somayajula, A., Falzarano, J.: Volterra GZ approach a new method to accurately calculate the non-linear and time-varying roll restoring arm of ships in irregular longitudinal seas. Ships and Offshore Structures **13**(4), 423–431 (2018). DOI 10.1080/17445302.

2017.1409457. URL https://www.tandfonline.com/doi/full/10.1080/17445302.2017.1409457
40. Somayajula, A., Falzarano, J., Lutes, L.: An Efficient Assessment of Vulnerability of a Ship to Parametric Roll in Irregular Seas using First Passage Statistics. Probabilistic Engineering Mechanics (Under Review) (2019)
41. Somayajula, A., Guha, A., Falzarano, J., Chun, H.H., Jung, K.H.: Added resistance and parametric roll prediction as a design criteria for energy efficient ships. Ocean Systems Engineering **4**(2), 117–136 (2014). DOI 10.12989/ose.2014.4.2.117. URL http://koreascience.or.kr/journal/view.jsp?kj=TPTPKZ{&}py=2014{&}vnc=v4n2{&}sp=117http://koreascience.or.kr/journal/view.jsp?kj=TPTPKZ{%}7B{&}{%}7Dpy=2014{%}7B{&}{%}7Dvnc=v4n2{%}7B{&}{%}7Dsp=117
42. Somayajula, A.S.: Reliability Assessment of Hull Forms Susceptible to Parametric Roll in Irregular Seas. Phd dissertation, Texas A&M University, College Station, TX (2017)
43. Somayajula, A.S., Falzarano, J.: A comparative assessment of simplified models for simulating parametric roll. Journal of Offshore Mechanics and Arctic Engineering **139**(2), 021103 (2017). DOI 10.1115/1.4034921. URL http://offshoremechanics.asmedigitalcollection.asme.org/article.aspx?doi=10.1115/1.4034921
44. Somayajula, A.S., Falzarano, J.M.: Non-linear dynamics of parametric roll of container ship in irregular seas. In: Proceedings of 33rd International Conference on Ocean, Offshore and Arctic Engineering - Volume 7: Ocean Space Utilization; Professor Emeritus J. Randolph Paulling Honoring Symposium on Ocean Technology, p. V007T12A018. ASME, San Francisco (2014). DOI 10.1115/OMAE2014-24186. URL http://proceedings.asmedigitalcollection.asme.org/proceeding.aspx?doi=10.1115/OMAE2014-24186
45. Somayajula, A.S., Falzarano, J.M.: Validation of Volterra series approach for modelling parametric rolling of ships. In: Proceedings of 34th International Conference on Ocean, Offshore and Arctic Engineering - Volume 11: Prof. Robert F. Beck Honoring Symposium on Marine Hydrodynamics, p. V011T12A043. ASME, St. John's, NL, Canada (2015). DOI 10.1115/OMAE2015-41467. URL http://proceedings.asmedigitalcollection.asme.org/proceeding.aspx?doi=10.1115/OMAE2015-41467
46. Spyrou, K.J.: Dynamic instability in quartering seas: The behavior of a ship during broaching. Journal of Ship Research **40**(1), 46–59 (1996). URL http://lib-ezproxy.tamu.edu:2048/login?url=http://search.ebscohost.com/login.aspx?direct=true{&}db=edselc{&}AN=edselc.2-52.0-0030104660{&}site=eds-live
47. Spyrou, K.J., Thompson, J.M.T.: Damping coefficients for extreme rolling and capsize An analytical approach. Journal of ship research **44**(1), 1–13 (2000). URL http://cat.inist.fr/?aModele=afficheN{&}cpsidt=13495001
48. Spyrou, K.J., Thompson, J.M.T.: The nonlinear dynamics of ship motions: a field overview and some recent developments. Philosophical Transactions of the Royal Society of London. Series A: Mathematical, Physical and Engineering Sciences **358**(1771), 1735–1760 (2000)
49. Su, Z.: Nonlinear response and stability analysis of vessel rolling motion in random waves using stochastic dynamical systems. Phd dissertation, Texas A&M University, College Station (2012). URL http://repositories.tdl.org/tdl-ir/handle/1969.1/ETD-TAMU-2012-08-11759
50. Su, Z., Falzarano, J.M.: Gaussian and non-Gaussian cumulant neglect application to large amplitude rolling in random waves. International Shipbuilding Progress **58**, 97–113 (2011). DOI 10.3233/ISP-2011-0071. URL http://iospress.metapress.com/index/L5K602364VW73W71.pdf
51. Su, Z., Falzarano, J.M.: Markov and Melnikov based methods for vessel capsizing criteria. Ocean Engineering **64**, 146–152 (2013). DOI 10.1016/j.oceaneng.2013.02.002. URL http://linkinghub.elsevier.com/retrieve/pii/S0029801813000826
52. Thompson, J.M.T., Rainey, R.C.T., Soliman, M.S.: Mechanics of ship capsize under direct and parametric wave excitation. Philosophical Transactions of the Royal Society A: Mathematical, Physical and Engineering Sciences **338**, 471–490 (1992). DOI 10.1098/rsta.1992.0015
53. Umeda, N., Francescutto, A.: Current state of the second generation intact stability criteria achievements and remaining issues. In: Proceedings of the 15th International Ship Stability Workshop, June, pp. 13–15. Stockholm, Sweden (2016)
54. Virgin, L.N.: The nonlinear rolling response of a vessel including chaotic motions leading to capsize in regular seas. Applied Ocean Research **9**(2), 89–95 (1987). DOI 10.1016/0141-1187(87)90011-3

55. Webster, W.: Motion in regular waves - Transverse motions. In: E. Lewis (ed.) Principles of Naval Architecture Vol III. SNAME, Jersey City (1989)
56. Wiggins, S.: Introduction to Applied Nonlinear Dynamical Systems and Chaos, 1st edn. Springer-Verlag, New York (1990)
57. Wiggins, S.: Introduction to Applied Nonlinear Dynamical Systems and Chaos, *Texts in Applied Mathematics*, vol. 2, 2nd edn. Springer-Verlag, New York (2003). DOI 10.1007/b97481. URL `http://link.springer.com/10.1007/b97481`
58. Wolf, A., Swift, J.B., Swinney, H.L., Vastano, J.A.: Determining Lyapunov exponents from a time series. Physica D: Nonlinear Phenomena **16**(3), 285–317 (1985). DOI 10.1016/0167-2789(85)90011-9
59. Zhu, W.Q.: Lyapunov exponent and stochastic stability of quasi-non-integrable Hamiltonian systems. International Journal of Non-Linear Mechanics **39**(4), 569–579 (2004). DOI 10.1016/S0020-7462(02)00223-8